Relation between interannual variations in satellite measures of northern forest greenness and climate between 1982 and 1999

L. Zhou,[1,2] R. K. Kaufmann,[1] Y. Tian,[1,2] R. B. Myneni,[1] and C. J. Tucker[3]

Received 6 May 2002; revised 29 July 2002; accepted 9 August 2002; published 3 January 2003.

[1] This paper analyzes the relation between satellite-based measures of vegetation greenness and climate by land cover type at a regional scale ($2^\circ \times 2^\circ$ grid boxes) between 1982 and 1999. We use the normalized difference vegetation index (NDVI) from the Global Inventory Monitoring and Modeling Studies (GIMMS) data set to quantify climate-induced changes in terrestrial vegetation. Climatic conditions are represented with monthly data for land surface air temperature and precipitation. The relation between NDVI and the climate variables is represented using a quadratic specification, which is consistent with the notion of a physiological optimum. The effects of spatial heterogeneity and unobserved variables are estimated with specifications and statistical techniques that allow coefficients to vary among grid boxes. Using this methodology, we are able to estimate statistically meaningful relations between NDVI and climate during spring, summer, and autumn for forests between 40°N and 70°N in North America and Eurasia. Of the variables examined, changes in temperature account for the largest fraction of the change in NDVI between the early 1980s and the late 1990s. Changes in stratospheric aerosol optical depth and precipitation have a smaller effect, while artifacts associated with variations in solar zenith angle are negligible. These results indicate that temperature changes between the early 1980s and the late 1990s are responsible for much of the observed increase in satellite measures of northern forest greenness. *INDEX TERMS:* 1615 Global Change: Biogeochemical processes (4805); 1620 Global Change: Climate dynamics (3309); 1640 Global Change: Remote sensing; *KEYWORDS:* NDVI, climate, greening, temperature, statistical techniques

Citation: Zhou, L., R. K. Kaufmann, Y. Tian, R. B. Myneni, and C. J. Tucker, Relation between interannual variations in satellite measures of northern forest greenness and climate between 1982 and 1999, *J. Geophys. Res.*, *108*(D1), 4004, doi:10.1029/2002JD002510, 2003.

1. Introduction

[2] Human activities change the atmospheric concentration and distribution of greenhouse gases and aerosols, and these changes may affect climate [*IPCC*, 2001]. The rate of temperature change during the past 25 years is greater than any previous period of the instrumental record. Warming is greatest in the northern high latitudes, especially during winter and spring [*Hansen et al.*, 1999]. This warming is associated with a reduction in the extent of sea ice and snow cover, and an earlier disappearance of snow in spring [*Groisman et al.*, 1994; *Vinnikov et al.*, 1999]. Precipitation also increases in the middle to high latitudes [*Easterling et al.*, 2000].

[3] Anthropogenic changes in climate may affect terrestrial ecosystems because climate and terrestrial ecosystems are closely coupled. Higher temperatures in the northern hemisphere may have increased the amplitude of the seasonal CO_2 cycle by about 30% since the early 1960s, which suggests an increase in terrestrial vegetation [*Keeling et al.*, 1995, 1996; *Randerson et al.*, 1999]. In the middle and high latitudes, warmer and wetter weather may increase net primary productivity by enhancing photosynthesis [*Kramer*, 1982; *Larcher*, 1983; *Chapin and Shaver*, 1996] or by enhancing nutrient availability through accelerated decomposition or mineralization [*Melillo et al.*, 1993].

[4] Spatial and temporal patterns of terrestrial vegetation have been closely linked with climate patterns [*Schultz and Halpert*, 1993]. The vegetation's response to climate change has been detected from seasonal and interannual variations in satellite measures of terrestrial vegetation [*Goward and Prince*, 1995; *Braswell et al.*, 1997]. *Myneni et al.* [1997] argue that terrestrial vegetation between 45°N and 70°N "greened" between 1981 and 1991. *Zhou et al.* [2001] found that this greening is tightly linked to changes in land surface temperature during the past two decades, which was reproduced from a biogeochemical model using observed climate data [*Lucht et al.*, 2002].

[5] This conclusion has an important socio-economic implication—warmer temperature may enhance plant growth in northern high latitudes and thereby affect the

[1]Department of Geography, Boston University, Boston, Massachusetts, USA.
[2]School of Earth and Atmospheric Sciences, Georgia Institute of Technology, Atlanta, Georgia, USA.
[3]Biospheric Sciences Branch, NASA Goddard Space Flight Center, Greenbelt, Maryland, USA.

0148-0227/02/2002JD002510$09.00

terrestrial carbon cycle [*Myneni et al.*, 2002]. It may be valid only at the continental scale. At the regional scale, continental relations may need to account for differences in vegetation types and lags in the relation between plant growth and temperature induced by biogeochemical feedbacks [*Braswell et al.*, 1997]. Analyses of surface greenness also must account for the effects of other factors that limit plant growth. For example, precipitation may be a more important factor than temperature in semiarid regions [*Myneni et al.*, 1996]. *Nemani et al.* [2002] suggest that increased rainfall and humidity spurred plant growth in the United States. In addition, artifacts associated with variations in aerosol optical depth and solar zenith angle may contaminate the satellite measures of vegetation greenness.

[6] Few studies have estimated quantitatively the relation between terrestrial vegetation and climate. To quantify the effects of climate and other variables on interannual variations in satellite measures of vegetation at the regional scale, we use statistical models to estimate the relation between the normalized difference vegetation index (NDVI) and climate by land cover type. To increase the reliability of the results, we use statistical techniques that; (1) account for the effects of unobserved variables and spatial heterogeneity on the relation between NDVI and climate, (2) reduce collinearity among explanatory variables, and (3) increase the degrees of freedom [*Hsiao*, 1986]. To separate the effect of climate on NDVI from possible artifacts in the satellite measures, the equations specify changes in solar zenith angle, which are associated with satellite drift and changeover, and changes in stratospheric aerosols, which are associated with volcanic eruptions.

[7] This paper has five sections. Section 2 describes how we compile data on satellite-based measures of NDVI, solar zenith angle, and stratospheric aerosol optical depth and ground-based measures of temperature and precipitation. The specifications used to estimate statistical models of the relation between NDVI and climate are consistent with the physiological mechanisms by which temperature and precipitation affect plant growth (section 3). For all forest land cover types in North America and Eurasia, there is a statistically meaningful relation among NDVI, climate, stratospheric aerosol optical depth, and solar zenith angle (section 4). Of these factors, temperature and stratospheric aerosol optical depth have the greatest effect on NDVI; the effect of changes in precipitation and solar zenith angle are smaller. Based on these results, section 5 concludes that changes in temperature account for the largest fraction of NDVI changes between the early 1980s and the late 1990s.

2. Data Set

[8] We assemble satellite and ground based data from 1982 to 1999 to examine the relation between satellite-based measures of vegetation greenness and climate by land cover type at a regional scale. These data are attached to a common spatial grid for North America and Eurasia between 40°N and 70°N. This latitudinal band is defined by (1) forest areas—where the nonvegetation effects of solar zenith angle are smaller relative to sparsely vegetated and barren regions [*Kaufmann et al.*, 2000]; (2) high latitudes—where temperature (and precipitation) probably are limiting factors [*Zhou et al.*, 2001]; and (3) quality of satellite data—where cloud cover is sparser than tropical areas. The sample period is defined by the availability of NDVI data (see below).

[9] NDVI can be used to proxy changes in terrestrial vegetation. NDVI is calculated from reflectances in channel 1 (0.58–0.68 μm) and channel 2 (0.73–1.1 μm), and is defined as

$$\mathrm{NDVI} = \frac{(\mathrm{Channel\ 2} - \mathrm{Channel\ 1})}{(\mathrm{Channel\ 2} + \mathrm{Channel\ 1})}. \quad (1)$$

NDVI measures the amount of energy absorbed by leaf pigments such as chlorophyll. As such, NDVI is closely correlated with the fraction of photosynthetically active radiation absorbed by plant canopies and therefore leaf area, leaf biomass, and potential photosynthesis [*Asrar et al.*, 1984; *Myneni et al.*, 1995].

[10] We use the 15-day NDVI and solar zenith angle (SZA) data set at 8 km resolution for the period January 1982 to December 1999 that is produced by the Global Inventory Monitoring and Modeling Studies (GIMMS) group from measurements of the advanced very high resolution radiometer (AVHRR) onboard the NOAA 7, NOAA 9, NOAA 11, and NOAA 14 satellites [*Zhou et al.*, 2001]. Data processing included improved navigation, sensor calibration, and atmospheric corrections for stratospheric aerosols [*Zhou et al.*, 2001]. Calibration based on data from high clouds and the dark ocean [*Vermote and Kaufman*, 1995] was first applied to the GIMMS reflectance data, and was then improved by using a sensor degradation correction method by *Los* [1998]. A time- and latitude-varying atmospheric correction [*Vermote and El Saleous*, 1994] was applied to the GIMMS NDVI data from April 1982 to December 1984 and from June 1991 to December 1993 to remove the effects of stratospheric aerosols from the El Chichon and Mt. Pinatubo eruptions. Such a correction tends to raise values for NDVI and has the greatest effect in the low latitudes.

[11] The raw AVHRR data include the effects of changes in sensor sensitivity (calibration problem) and satellite orbital drift, which changes Sun-target-sensor geometry. The effects of orbital drift always are combined with the effects of absorption and scattering due to ozone, water vapor, Rayleigh scattering, atmospheric aerosols, and surface anisotropy [*Gutman*, 1999]. Their effects on reflectance in the visible and near-infrared wavelengths, which are used to calculate NDVI and surface bidirectional effects, are determined by properties of both the surface and atmosphere that vary over space and time. Although these effects have been examined extensively, removing these nonvegetation effects from data with global coverage remains a challenge because it involves the closure of a system of radiance equations with many more unknowns than measurable quantities.

[12] Nonvegetation effects are reduced by analyzing only the maximum NDVI value within each 15-day interval, which is termed compositing [*Holben*, 1986]. Compositing the maximum value of NDVI reduces but does not eliminate, residual atmospheric and bidirectional effects. The quality of the GIMMS NDVI data set between 40°N and 70°N is assessed by *Zhou et al.* [2001]. Their analysis indicates that the data are of satisfactory quality.

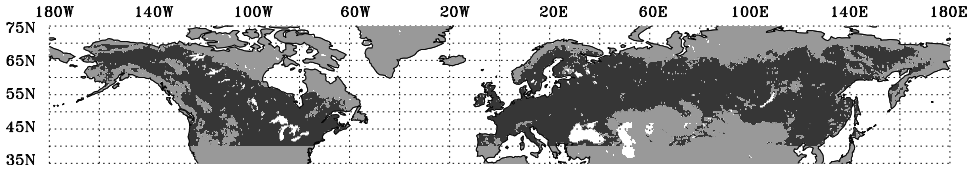

Figure 1. Map of vegetated pixels used in this study. Vegetated pixels (solid) are identified as those with (a) June to August NDVI composite values greater than 0.1 in all years; and (b) June to August average NDVI value greater than 0.3 for all years, from 1982 to 1999.

[13] However, the GIMMS NDVI still may contain variations due to orbital drift and incomplete corrections for calibration loss and atmospheric effects. No explicit atmospheric corrections are applied to the GIMMS data. Nor are corrections made for changes in Sun-target-sensor geometry, the so-called SZA effect. This effect varies by latitude, season and land cover [*Gutman*, 1999]. Theoretical and empirical analyses indicate that the SZA effects on NDVI decrease as SZA decreases and/or leaf area increases [*Huemmrich et al.*, 1999; *Kaufmann et al.*, 2000]. This implies that the SZA effect on forest NDVI should be small. Nonetheless, changes in SZA may account for some portion of the interannual variations in NDVI, especially at the regional scale. To capture this potential effect, SZA is included in the regression equations (see section 3).

[14] To reduce the SZA effect on NDVI and to exclude artifacts introduced by variability in soil background, we analyze relatively dense vegetated pixels only. We define "vegetated pixels" (Figure 1) as those with: (1) June to August NDVI values greater than 0.1 in all years; and (2) June to August average NDVI value greater than 0.3 for all years. Winter season NDVI data (January, February, March, November, December) are excluded to reduce nonvegetation effects, especially those associated with snow and low solar elevation, which are typical in high latitudes. This definition for vegetated pixels also ensures that data from the same pixels are used in the entire analysis unlike *Myneni et al.* [1997].

[15] To measure conditions experienced by terrestrial vegetation, we use monthly data for land surface air temperature and precipitation from 1982 to 1999. The temperature data set is processed by the NASA Goddard Institute for Space Studies (GISS) [*Hansen et al.*, 1999] and has a resolution of $2^\circ \times 2^\circ$. The temperature value reported for each grid box is an average of measurements recorded at stations in rural areas, small towns, and urban areas. Measurements from urban stations are adjusted so their long-term trend matches that of their rural neighbors. The station data are collected by national meteorological services and are reported by the Global Historical Climatology Network of *Peterson and Vose* [1997]. Temperature data are reported as anomalies relative to the 1951–1980 mean. The precipitation data are from the NOAA Climate Prediction Center and have a resolution of $2.5^\circ \times 2.5^\circ$ [*Xie and Arkin*, 1997]. This data set is produced by merging measurements from ground-based precipitation gauges, satellite estimates, and numerical model predictions.

[16] Aerosol scattering affects reflectances in both the visible and near-infrared channels. Increases in atmospheric optical depth of tropospheric and stratospheric aerosols reduce NDVI. Quantitative characteristics of tropospheric aerosols are insufficient because they are spatially and temporally variable [*Gutman*, 1999]. Stratospheric aerosols associated with volcanic eruptions, however, tend to have longitudinally homogeneous distributions within two months of injection and decrease slowly with time. The availability of stratospheric aerosol data makes it possible to correct the GIMMS NDVI data for the effect of aerosols associated with volcanic eruptions. The stratospheric aerosol optical depth (AOD) data we use are based on optical extinction measurements from the Stratospheric Aerosol and Gas Experiment (SAGE) satellite instruments [*Sato et al.*, 1993], and are reported as monthly values for zonal means. That is, AOD varies by latitude, but is constant across longitudes. We use these AOD data from 1982 to 1999 [*Sato et al.*, 1993] to assess the effect of changes in aerosol optical depth on the GIMMS NDVI time series that may remain after corrections.

[17] We use a land cover classification map with an 8 km resolution [*DeFries et al.*, 1998] to identify vegetated pixels by land cover type. This map is derived from AVHRR data and identifies 13 land cover types in North America and Eurasia (Table 1). Of the 13 land cover types, this statistical analysis includes five (evergreen needleleaf forests—class 1; deciduous needleleaf forests—class 3; deciduous broadleaf forests—class 4; mixed forests—class 5; and woodlands—class 6). The remaining land cover types are excluded because they are not present in the sample area (evergreen broadleaf forests—class 2), are managed by humans (croplands—class 11), or contain little vegetation relative to forests (wooded grasslands/shrublands—class 7; closed bushlands or shrublands—class 8; open shrubs—class 9; grasses—class 10; bare—class 12; and mosses and lichens—class 13).

Table 1. Distribution of Vegetated Pixels Between 40°N and 70°N for Each Land Cover Type in North America and Eurasia

Class	Land Cover Type Description	North America		Eurasia	
		Pixels	Percent	Pixels	Percent
1	Evergreen needleleaf forests	50,989	34.9	68,394	21.5
2	Evergreen broadleaf forests	0	0.0	0	0.0
3	Deciduous needleleaf forests	0	0.0	30,779	9.7
4	Deciduous broadleaf forests	6846	4.7	18,060	5.7
5	Mixed forests	19,145	13.1	38,249	12.0
6	Woodlands	23,835	16.3	22,882	7.2
7	Wooded grasslands/shrubs	151	0.1	1057	0.3
8	Closed bushlands or shrublands	109	0.1	415	0.1
9	Open shrublands	512	0.4	638	0.2
10	Grasses	16,388	11.2	51,045	16.1
11	Croplands	18,657	12.8	63,800	20.1
12	Bare	0	0.0	4	0.0
13	Mosses and lichens	9408	6.4	22,698	7.10
Total		146,040	100.0	318,021	100.0

[18] We generate anomalies for the time series of NDVI, SZA, AOD, and climate variables by subtracting the 18-year averaged annual cycle [*Zhou et al.*, 2001]. Anomalies are less correlated across space [*Hansen et al.*, 1999] and therefore their use eliminates spatial trends that can create/enhance correlations among data. That is, the R^2 for regression equations are lower than had levels been used. As a result, specifying anomalies reduces the R^2 for the regression equations described in section 3.

[19] Due to the large number of vegetated pixels (tens of millions), we aggregate observations over space and time. An area-weighted average is used for spatial and temporal aggregation. Because climate data, AOD, and NDVI are reported at different spatial resolutions, we first generate climate data at the 8 km resolution. Each grid of climate data is considered to be a square cell with a single value for climate. We interpolate the climate data from the original large scale to the 8 km resolution of the GIMMS NDVI/SZA data. That is, all vegetated pixels in a grid box are assigned the same values for temperature and precipitation. AOD data are processed similarly. NDVI, SZA, AOD, and climate variables for vegetated pixels are then georeferenced to the $2^\circ \times 2^\circ$ grid. In each grid box, the 8 km pixel values for all data are classified by land cover type—Pixels that belong to the same land cover type are averaged to generate values for each land cover type.

[20] The data also are averaged temporally. Values for the 15-day composite of NDVI and SZA are averaged to generate monthly values. Monthly data are then averaged to generate seasonal values; spring (April, May), summer (June, July, August), and autumn (September, October). Unlike NDVI, climate data for winter months (January, February, March) are included in the statistical models.

3. Modeling the Relation Between NDVI and Climate

[21] The general relation between NDVI and climate is modeled by

$$\mathrm{NDVI} = \alpha + \beta_1 \mathrm{Temp} + \beta_2 \mathrm{Temp}^2 + \beta_3 \mathrm{Prec} + \beta_4 \mathrm{Prec}^2 + \beta_5 \mathrm{SZA} + \beta_6 \mathrm{AOD} + \varepsilon, \quad (2)$$

in which NDVI, Temp, Prec, SZA, and AOD are the seasonal anomaly for NDVI, temperature, precipitation, solar zenith angle, and stratospheric aerosol optical depth, respectively, α, β_1–β_6 are coefficients that are estimated statistically, and ε is the unexplained regression error.

[22] The relation between NDVI and the climate variables is represented using a quadratic specification. This specification is consistent with the notion of a physiological optimum—the maximum rate of net primary productivity may occur at an intermediate temperature or precipitation. This effect would be consistent with a positive value for the regression coefficient associated with the linear value of the climate variable (β_1, β_3) and a negative value associated with the squared value of the climate variable (β_2, β_4). Using a quadratic relation to represent the effect of a physiological optimum is consistent with statistical models for the effect of climate on crop yield [*Kaufmann and Snell*, 1997].

[23] Representing the effect of climate on NDVI with a quadratic specification, instead of a simple linear function, also is consistent with physiological studies. Warmer temperatures increase the growth rates of most plants, particularly near the center of their climate ranges, provided water and nutrients are available. Warming beyond a certain point will reduce growth and may cause dieback [*Gates*, 1993]. In addition, plants can shift their photosynthetic optimum toward higher temperatures when they are grown under warmer conditions. This results from a shift in the enzyme systems that affect both photosynthesis and respiration. Seasonal shifts in the optimal temperature are found in some evergreen plants. These shifts in temperature optima may be only a few degrees; nevertheless, they are effective means of adjustment to changing climates [*Larcher*, 1983].

[24] Equation (2) does not impose an inverted U shape on the relation between NDVI and climate. Four other relations are possible. There is a positive relation between NDVI and climate if the regression coefficients associated with the linear and/or squared value of the climate variable is positive and statistically significant. There is a negative relation if the regression coefficients associated with the linear and/or squared value of the climate variable is negative and statistically significant. There is a U-shaped relation if the regression coefficient associated with the linear value of the climate variable is negative (and statistically significant) and the regression coefficient associated with the squared value of the climate variable is positive (and statistically significant). Finally, there is no relation between NDVI and climate if the regression coefficients associated with the linear and squared value of the climate variables are not statistically significant. Their signs are irrelevant if the regression coefficients are not statistically significant.

[25] Equation (2) includes the variables SZA and AOD to represent the effects of satellite orbital drift and changover, and stratospheric aerosols that are not removed by the GIMMS NDVI processing algorithms. It is not possible to determine the sign on these regression coefficients (β_5, β_6) a priori. Increases in stratospheric aerosol optical depth reduce NDVI, but β_6 will not be negative if the corrections for the El Chichon and Mt. Pinatubo eruptions are too large. By including SZA and AOD, the coefficients associated with temperature and precipitation represent the effects of climate that are not correlated with the effects of orbital drift, satellite changeover, or aerosol optical depth.

[26] Using equation (2) to estimate the relation between NDVI and climate from the 18 years of data for the 445 grid boxes in North America and the 980 grid boxes in Eurasia presents several difficulties. First, NDVI in any given season may be determined by climate during an earlier portion of the growing season. That is, NDVI during the summer may be determined by temperature during both the summer and spring. As a result, we expand equation (2) to include the effect of climate variables during earlier portions of the growing season. We include two previous seasons (except for spring when we include spring and winter climate variables only) to conserve degree of freedom for the random coefficient model (see below).

[27] In addition, equation (2) assumes that the relation between NDVI and climate for a given land cover type is the same across all grid boxes. This assumption may not be

consistent with physiological and ecological mechanisms. Acclimatization and local selection may cause the effect of temperature and/or precipitation on NDVI to differ between the northern and southern portion of a species range. In addition, unobserved variables that are not related to climate or the other variables in equation (2) may cause the relation between NDVI and climate to vary among grid boxes. Differences in surface features such as elevation and slope may cause the satellite to measure different reflectances in channels 1 and/or 2 even if the vegetation is identical. These effects are represented by allowing the regression coefficients to vary across grid boxes.

[28] The effects of temporal lags, spatial heterogeneity, and unobserved variables can be represented several ways. We can add the effect of lagged climate variables but keep the relation between NDVI and climate the same across grid boxes by

$$\mathrm{NDVI}_{\mathrm{sit}} = \alpha + \sum_{s=0}^{-2} \left(\beta_{\mathrm{s}1}\mathrm{Temp}_{\mathrm{sit}} + \beta_{\mathrm{s}2}\mathrm{Temp}_{\mathrm{sit}}^2 + \beta_{\mathrm{s}3}\mathrm{Prec}_{\mathrm{sit}} + \beta_{\mathrm{s}4}\mathrm{Prec}_{\mathrm{sit}}^2\right) + \beta_{\mathrm{s}5}\mathrm{SZA}_{\mathrm{sit}} + \beta_{\mathrm{s}6}\mathrm{AOD}_{\mathrm{sit}} + \varepsilon_{\mathrm{sit}}, \quad (3)$$

in which s represents season (winter, spring, summer, autumn), i represents an individual grid box, and t is time. Alternatively, we can represent the effect of unobserved variables by allowing the intercepts to vary (α_{i}) among grid boxes by

$$\mathrm{NDVI}_{\mathrm{sit}} = \alpha_{\mathrm{i}} + \sum_{s=0}^{-2} \left(\beta_{\mathrm{s}1}\mathrm{Temp}_{\mathrm{sit}} + \beta_{\mathrm{s}2}\mathrm{Temp}_{\mathrm{sit}}^2 + \beta_{\mathrm{s}3}\mathrm{Prec}_{\mathrm{sit}} + \beta_{\mathrm{s}4}\mathrm{Prec}_{\mathrm{sit}}^2\right) + \beta_{\mathrm{s}5}\mathrm{SZA}_{\mathrm{sit}} + \beta_{\mathrm{s}6}\mathrm{AOD}_{\mathrm{sit}} + \varepsilon_{\mathrm{sit}}. \quad (4)$$

Finally, we can represent spatial heterogeneity by allowing the coefficients (β_1–β_6) to vary among grid boxes by

$$\mathrm{NDVI}_{\mathrm{sit}} = \alpha_{\mathrm{i}} + \sum_{s=0}^{-2} \left(\beta_{\mathrm{si}1}\mathrm{Temp}_{\mathrm{sit}} + \beta_{\mathrm{si}2}\mathrm{Temp}_{\mathrm{sit}}^2 + \beta_{\mathrm{si}3}\mathrm{Prec}_{\mathrm{sit}} + \beta_{\mathrm{si}4}\mathrm{Prec}_{\mathrm{sit}}^2\right) + \beta_{\mathrm{si}5}\mathrm{SZA}_{\mathrm{sit}} + \beta_{\mathrm{si}6}\mathrm{AOD}_{\mathrm{sit}} + \varepsilon_{\mathrm{sit}}. \quad (5)$$

There is no way to choose among equations (3)–(5) a priori. Instead, we use standard statistical procedures to choose the equation that is consistent with the data, the proper technique to estimate the equation, and the way to evaluate results [*Hsiao*, 1986]. A flowchart for these procedures is given in Figure 2.

[29] The procedure to choose among equations (3), (4), and (5) is based on *F* tests which are presented in more detailed in Appendix A. Once equation (3), (4), or (5) is chosen, each requires a different estimation technique. Equation (3) can be estimated using ordinary least squares (OLS). In case of heteroscedasticity, weighted least squares (WLS) can be used to eliminate the heteroscadasticity if its cause is known. Possible causes include differences among grid boxes concerning the number of vegetated pixels. Otherwise, a heteroscedactic and autocorrelation consistent (HAC) estimator is used. Equation (4) can be estimated using either the fixed or the random effects estimator. If the *F* tests indicate that both the intercepts and slopes vary among grid boxes, we estimate equation (5) using the random coefficient model (RCM).

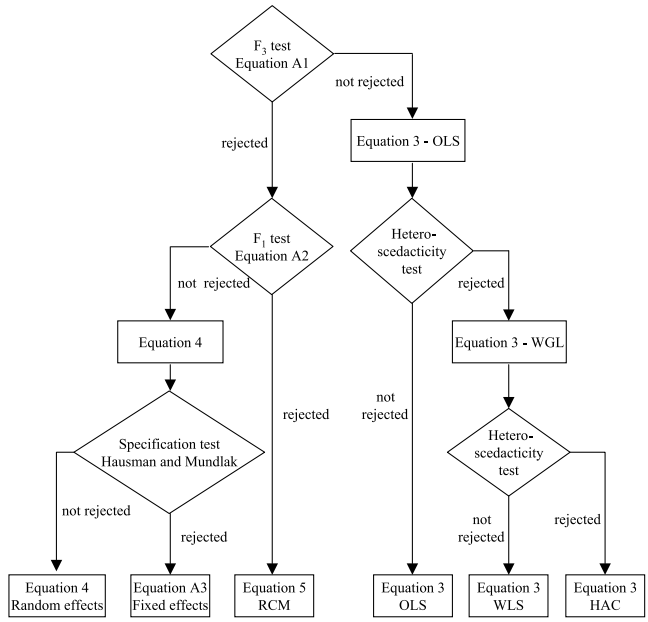

Figure 2. Flowchart of statistical methods.

[30] Finally, we test the results for the presence of spurious regressions. Spurious regressions generate diagnostic statistics (e.g., *t* statistics for the β's) that suggest a statistically meaningful relation among variables when none is present. To avoid such confusion, we use two Dickey–Fuller (DF_ρ^*, DF_t^*) tests and an augmented Dickey–Fuller (ADF) test to test the null hypothesis of no cointegration [*Kao*, 1999]. Simulation results suggest that the DF_ρ^* and DF_t^* tests can be used for regression residuals with small standard errors, and the ADF test is suited for regression residuals with large standard errors. To evaluate the degree to which the results are robust, we report all three tests.

4. Results

[31] We are able to estimate statistically meaningful relations between NDVI and climate during spring, summer, and autumn for all forest land cover types in North America and Eurasia (Tables 2, 3, and 4). In each of the 27 regression equations, one or more of the climate variables is statistically significant at $p < 0.05$ (Table 5). For only 12 climate variables of the 144 tested, are both the linear and squared term statistically insignificant (i.e. no relation between NDVI and climate). Of the 51 cointegration tests, 50 statistics are significant, that is, the null hypothesis of no cointegration is rejected. This implies that the variables in the regressions probably cointegrate and the regression results probably are not spurious. Nonetheless, this conclusion must be interpreted with caution. The tests developed by *Kao* [1999] are designed for fixed effects estimator. As such, the tests are applicable to models estimated using OLS because NDVI and the independent variables are specified as anomalies, which is the same transformation used to estimate the fixed effect estimator. The residual from

Table 2. Regression Results for Equations (3), (4), or (5) for Spring

	Land Cover Types				
	1	3	4	5	6
	North America				
Regression coefficients[a]					
T (winter)	.0052[b]	–	.0061[b]	.0064[b]	.0023[b]
T^2 (winter)	−.0006[b]	–	−.0004[b]	−.0007[b]	−.0006[b]
T (spring)	.0079[b]	–	.0087[b]	.0099[b]	.0040[b]
T^2 (spring)	−.0007[b]	–	.0011[b]	.0003	−.0005[b]
P (winter)	−.0090[b]	–	−.0169[b]	−.0086[b]	−.0037[b]
P^2 (winter)	.0037[b]	–	.0380[b]	−.0004	.0058[b]
P (spring)	−.0041[b]	–	−.0020[b]	−.0045[b]	−.0021[b]
P^2 (spring)	.0026[b]	–	.0040[b]	.0079[b]	.0009
SZA	.0006[b]	–	.0000	.0004[b]	.0007[b]
AOD	−.1605[b]	–	−.1677[b]	−.1828[b]	−.0901[b]
Diagnostic statistics[c]					
DF_ρ^*	−38.83[b]	–	−52.26[b]	−41.43[b]	−41.81[b]
DF_t^*	−4.55[b]	–	−17.45[b]	−7.79[b]	−11.64[b]
ADF	−10.61[b]	–	−13.50[b]	−9.84[b]	−10.28[b]
R^2	0.31	–	0.19	0.35	0.09
Degrees of freedom					
	1911	–	910	1246	714
Estimator[d]	RCM	–	RCM	RCM	RCM
	Eurasia				
Regression coefficients[a]					
T (winter)	.0020[b]	.0008[b]	.0051[b]	.0032[b]	.0005[b]
T^2 (winter)	−.0004[b]	−.0003[b]	−.0009[b]	−.0006[b]	−.0002[b]
T (spring)	.0013[b]	.0006[b]	.0046[b]	.0027[b]	.0006[b]
T^2 (spring)	.0005[b]	.0004[b]	.0006[b]	.0008[b]	.0003[b]
P (winter)	−.0035[b]	−.0061[b]	−.0067[b]	−.0044[b]	.0008
P^2 (winter)	.0004	.0246[b]	.0046[b]	.0050[b]	.0015
P (spring)	−.0046[b]	−.0058[b]	−.0020[b]	−.0048[b]	−.0040[b]
P^2 (spring)	−.0019[b]	−.0009	−.0032	−.0029[b]	.0015
SZA	.0000	.0008[b]	−.0003[b]	.0000	.0008[b]
AOD	−.1078[b]	−.0699[b]	−.1120[b]	−.1163[b]	−.0830[b]
Diagnostic statistics[c]					
DF_ρ^*	−39.32[b]	−36.84[b]	−46.34[b]	−46.97[b]	−46.18[b]
DF_t^*	−1.16	−5.67[b]	−5.64[b]	−4.38[b]	−10.39[b]
ADF	−8.40[b]	−8.51[b]	−10.29[b]	−10.33[b]	−10.31[b]
R^2	0.15	0.12	0.19	0.17	0.06
Degrees of freedom					
	4004	1246	2149	2982	1274
Estimator[d]	RCM	RCM	RCM	RCM	RCM

[a] T = temperature; P = precipitation; SZA = solar zenith angle; AOD = stratospheric aerosol optical depth. These coefficients are estimated regression coefficients, β_1–β_6, for equations (3)–(5).

[b] Values that exceed the critical values for a threshold of $p < .05$.

[c] DF_ρ^*, DF_t^*, and ADF are Dickey–Fuller tests and augmented Dickey–Fuller test proposed by *Kao* [1999]. These tests are used to test whether the regression is spurious. The null hypothesis is no cointegration.

[d] RCM = random coefficient model. See Appendix A and Figure 2 for details.

the random coefficient model also are tested for no cointegration using the Kao statistics because no cointegration test has been developed for this estimation technique. We believe that the results are informative because in most cases the test statistic strongly rejects the null hypothesis ($p < 0.001$) and so the conclusions about cointegration probably are robust.

[32] The F tests indicate that the relation between NDVI and climate should be estimated using either equation (3) (12 relations) or equation (5) (15 relations) (Tables 2–4). The use of equation (3) as opposed to equation (4) is consistent with the use of NDVI and climate anomalies instead of levels. The anomalies are created with a transformation similar to that used to calculate the fixed effects estimator. This similarity implies that the intercepts vary among all land cover types, even those for which the relation between NDVI and climate is estimated using equation (3). For all uses of equation (3), we report the HAC estimate. In no case, do we choose the estimate generated by weighted least squares. This indicates that the OLS estimate of equation (3) generates an error term

Table 3. Regression Results for Equations (3), (4), or (5) for Summer

	Land Cover Types				
	1	3	4	5	6
	North America				
Regression coefficients[a]					
T (winter)	.0021[b]	–	.0041[b]	.0037[b]	.0015[b]
T^2 (winter)	−.0005[b]	–	−.0010[b]	−.0010[b]	−.0006[b]
T (spring)	.0005[b]	–	.0006[b]	.0011[b]	.0018[b]
T^2 (spring)	.0001	–	.0001	.0001	.0000
T (summer)	.0055[b]	–	.0001	.0004	.0059[b]
T^2 (summer)	.0012[b]	–	.0014[b]	.0009[b]	.0004[b]
P (winter)	−.0016[b]	–	−.0009	.0000	−.0032[b]
P^2 (winter)	.0007	–	−.0014[b]	−.0002	.0008
P (spring)	.0031[b]	–	.0020[b]	.0023[b]	.0008
P^2 (spring)	−.0009	–	.0007	−.0059	.0043
P (summer)	−.0051[b]	–	−.0007	−.0030[b]	−.0026[b]
P^2 (summer)	−.0006	–	−.0045[b]	−.0058[b]	−.0005
SZA	−.0010[b]	–	−.0007[b]	−.0009[b]	−.0006[b]
AOD	−.1545[b]	–	−.1996[b]	−.1553[b]	−.1751[b]
Diagnostic statistics[c]					
DF_ρ^*	−50.14[b]	–	−49.11[b]	−52.50[b]	−56.09[b]
DF_t^*	−8.56[b]	–	−12.26[b]	−12.79[b]	−12.38[b]
ADF	−11.96[b]	–	−12.99[b]	−13.54[b]	−11.83[b]
R^2	0.21	–	0.16	0.17	0.25
Degrees of freedom					
	1083	–	570	678	876
Estimator[d]	RCM	–	RCM	RCM	RCM
	Eurasia				
Regression coefficients[a]					
T (winter)	.0028[b]	.0016[b]	.0027[b]	.0030[b]	.0024[b]
T^2 (winter)	−.0005[b]	−.0001	−.0004[b]	−.0005[b]	−.0002[b]
T (spring)	−.0007[b]	.0022[b]	−.0011[b]	−.0009[b]	.0001
T^2 (spring)	.0005[b]	.0000	.0004[b]	.0005[b]	.0002[b]
T (summer)	.0078[b]	.0106[b]	.0050[b]	.0067[b]	.0106[b]
T^2 (summer)	−.0009[b]	.0005	−.0009[b]	−.0008[b]	−.0010[b]
P (winter)	.0004	−.0017	−.0007	−.0005	−.0012
P^2 (winter)	.0001	−.0114[b]	−.0002	.0000	.0005
P (spring)	.0088[b]	.0019	.0095[b]	.0073[b]	.0081[b]
P^2 (spring)	−.0034[b]	−.0008	−.0029[b]	−.0026[b]	−.0051[b]
P (summer)	−.0036[b]	−.0005	−.0020[b]	−.0057[b]	−.0024[b]
P^2 (summer)	−.0025[b]	−.0087[b]	−.0031[b]	−.0026[b]	−.0033[b]
SZA	−.0009[b]	−.0006[b]	−.0007[b]	−.0010[b]	−.0006[b]
AOD	−.1861[b]	−.1250[b]	−.2165[b]	−.1817[b]	−.1747[b]
Diagnostic statistics[c]					
DF_ρ^*	−57.72[b]	−39.66[b]	−61.44[b]	−54.00[b]	−64.04[b]
DF_t^*	−6.15[b]	−3.85[b]	−11.00[b]	−6.46[b]	−10.50[b]
ADF	−11.99[b]	−9.27[b]	−13.27[b]	−11.93[b]	−13.73[b]
R^2	0.24	0.24	0.17	0.23	0.23
Degrees of freedom					
	12,009	5961	7437	9453	9165
Estimator[e]	HAC	HAC	HAC	HAC	HAC

[a] T = temperature; P = precipitation; SZA = solar zenith angle; AOD = stratospheric aerosol optical depth. These coefficients are estimated regression coefficients, β_1–β_6, for equations (3)–(5).

[b] Values that exceed the critical values for a threshold of $p < .05$.

[c] DF_ρ^*, DF_t^*, and ADF are Dickey–Fuller tests and augmented Dickey–Fuller test proposed by *Kao* [1999]. These tests are used to test whether the regression is spurious. The null hypothesis is no cointegration.

[d] RCM = random coefficient model. See Appendix A and Figure 2 for details.

[e] HAC = heteroscedactic and autocorrelation model. See Appendix A and Figure 2 for details.

Table 4. Regression Results for Equations (3), (4), or (5) for Autumn

	Land Cover Types				
	1	3	4	5	6
	North America				
Regression coefficients[a]					
T (spring)	−.0022[b]	–	−.0055[b]	−.0046[b]	−.0007
T^2 (spring)	−.0001	–	.0003	−.0002	−.0002
T (summer)	−.0027[b]	–	−.0035[b]	−.0013	−.0013[b]
T^2 (summer)	.0010[b]	–	.0022[b]	.0011[b]	−.0001
T (autumn)	.0036[b]	–	.0057[b]	.0058[b]	.0021[b]
T^2 (autumn)	−.0009[b]	–	.0003	.0003	−.0016[b]
P (spring)	−.0005	–	−.0035[b]	−.0023[b]	.0035[b]
P^2 (spring)	.0004	–	.0016	.0001	.0006
P (summer)	.0017[b]	–	.0070[b]	.0030[b]	.0027[b]
P^2 (summer)	−.0005	–	−.0005	−.0001	−.0039[b]
P (autumn)	−.0053[b]	–	−.0048[b]	−.0060[b]	−.0064[b]
P^2 (autumn)	.0002	–	−.0004	−.0005	.0007[b]
SZA	−.0030[b]	–	−.0028[b]	−.0031[b]	−.0030[b]
AOD	−.2116[b]	–	−.2395[b]	−.1691[b]	−.2437[b]
Diagnostic statistics[c]					
DF_ρ^*	−47.98[b]	–	−49.97[b]	−57.92[b]	−57.53[b]
DF_t^*	−6.96[b]	–	−11.43[b]	−14.77[b]	−13.08[b]
ADF	−12.80[b]	–	−10.98[b]	−12.28[b]	−11.63[b]
R^2	0.33	–	0.33	0.31	0.31
Degrees of freedom					
	6375	–	3351	4017	4935
Estimator[d]	HAC	–	HAC	HAC	HAC
	Eurasia				
Regression coefficients[a]					
T (spring)	.0029[b]	−.0025[b]	−.0025[b]	−.0033[b]	−.0024[b]
T^2 (spring)	−.0006[b]	−.0007[b]	−.0007[b]	.0001	.0000
T (summer)	−.0009[b]	−.0014[b]	−.0014[b]	.0005	.0022[b]
T^2 (summer)	.0006[b]	.0075[b]	.0075[b]	.0038[b]	.0005
T (autumn)	.0058[b]	.0049[b]	.0049[b]	.0049[b]	.0046[b]
T^2 (autumn)	−.0008[b]	.0007[b]	.0007[b]	−.0003	−.0003
P (spring)	.0003	.0029[b]	.0029[b]	.0021[b]	−.0004
P^2 (spring)	.0002	−.0055[b]	−.0055[b]	−.0035[b]	−.0005
P (summer)	.0068[b]	.0065[b]	.0065[b]	.0015[b]	.0020[b]
P^2 (summer)	−.0021[b]	−.0006	−.0006	−.0007	−.0021
P (autumn)	−.0027[b]	−.0120[b]	−.0120[b]	−.0120[b]	−.0191[b]
P^2 (autumn)	−.0016[b]	.0021[b]	.0021[b]	−.0002	.0008
SZA	−.0011[b]	−.0032[b]	−.0032[b]	−.0037[b]	−.0034[b]
AOD	−.2236[b]	−.2594[b]	−.2594[b]	−.2215[b]	−.2863[b]
Diagnostic statistics[c]					
DF_ρ^*	−67.28[b]	−47.73[b]	−64.15[b]	−70.56[b]	−74.44[b]
DF_t^*	−9.64[b]	−6.65[b]	−12.47[b]	−13.23[b]	−15.23[b]
ADF	−15.69[b]	−12.50[b]	−14.66[b]	−16.21[b]	−17.20[b]
R^2	0.27	0.30	0.30	0.32	0.29
Degrees of freedom					
	7123	921	1224	9363	8427
Estimator[e]	HAC	RCM	RCM	HAC	HAC

[a] T = temperature; P = precipitation; SZA = solar zenith angle; AOD = stratospheric aerosol optical depth. These coefficients are estimated regression coefficients, β_1–β_6, for equations (3)–(5).

[b] Values that exceed the critical values for a threshold of $p < .05$.

[c] DF_ρ^*, DF_t^*, and ADF are Dickey–Fuller tests and augmented Dickey–Fuller test proposed by *Kao* [1999]. These tests are used to test whether the regression is spurious. The null hypothesis is no cointegration.

[d] HAC = heteroscedactic and autocorrelation consistent. See Appendix A and Figure 2 for details.

[e] HAC = heteroscedactic and autocorrelation consistent; RCM = random coefficient model. See Appendix A and Figure 2 for details.

that does not have constant variance and that the cause of this heteroscedasticity is not related to differences among grid boxes regarding the number of pixels that belong to a given land cover type.

[33] Of the 72 temperature variables in the 27 regression equations, 25 temperature variables have an inverted U shape relation with NDVI (Table 5). This shape is consistent with the notion of a physiological optimum. The absolute value of this optimum cannot be calculated from the regression coefficients because the variables are specified as anomalies rather than the levels. For the remaining 47 temperature variables, there are 29 positive relations between NDVI and temperature. This positive relation is consistent with the observation that temperature is a limiting factor for many land cover types located between 40°N and 70°N. The number of negative relations between NDVI and temperature is limited. Of these, most occur in the equations for autumn NDVI. Six temperature variables have a U shaped relation with NDVI. In these cases, the turning point (i.e., trough) tends to be located near the sample maximum or minimum value. This implies that the U shaped relation may actually represent an asymptotic negative or positive effect.

[34] The relation between NDVI and precipitation shows a different mix of relations. Twenty-nine precipitation variables have a negative effect on NDVI (Table 5). For 11 precipitation variables, there is no statistically meaningful relation with NDVI. There is a U shaped relation and a positive relation between NDVI and precipitation for 12 precipitation variables, respectively. There are 8 precipitation variables for Eurasia that have an inverted U shaped relation with NDVI while there are no inverted U shaped relations in North America.

[35] For all land cover types and seasons, there is a negative relation between NDVI and AOD. The statistical significance of this relation indicates that the algorithm used to process the GIMMS data set does not eliminate the effects of the El Chichon and Mt. Pinatubo eruptions. The negative sign indicates that the effect of aerosols on NDVI is greater than that assumed by the GIMMS NDVI processing algorithm.

[36] As noted in section 2, the processing algorithm does not include corrections for changes in SZA. This omission generates a statistically significant relation between NDVI and SZA for most land cover types and seasons. The nature of this relation varies among seasons. There is a positive relation between NDVI and SZA during the spring and a

Table 5. Summary of Relation Between NDVI and Climate Variables From Tables 2–4 for North America and Eurasia[a]

	Spring		Summer		Autumn		Total		
Relation	NA	EA	NA	EA	NA	EA	NA	EA	Total
				Temperature					
Inverted U	6	5	4	8	0	2	10	15	25
Positive	2	5	8	4	4	6	14	15	29
Negative	0	0	0	3	4	4	4	7	11
U Shaped	0	0	0	0	3	3	3	3	6
No relation	0	0	0	0	1	0	1	0	1
Total	8	10	12	15	12	15	32	40	72
				Precipitation					
Inverted U	0	0	0	4	0	4	0	8	8
Positive	0	0	4	0	4	4	8	4	12
Negative	2	6	6	6	6	3	14	15	29
U Shaped	6	3	0	0	1	2	7	5	12
No relation	0	1	2	5	1	2	3	8	11
Total	8	10	12	15	12	15	32	40	72

[a] NA = North America; EA = Eurasia.

negative relation during the summer and autumn. The reason for these seasonal differences is unknown.

[37] The presence of a statistically meaningful relation among NDVI, climate, SZA, and AOD does not mean that the NDVI data are 'hopelessly contaminated' by the changes in SZA and AOD. By including these variables in the regression equation, the statistical techniques are able to quantify the effects of SZA and AOD that remain in the GIMMS NDVI data set and thereby separate their effects from the effects of climate. As indicated in the next section, the effects of SZA are small compared with climate.

5. Discussion

[38] As first described by *Zhou et al.* [2001], NDVI generally increases between the early 1980s and the late 1990s (Figures 3a, 3b, and 3c). Nevertheless, the direction and magnitude of changes vary over space and time. In Eurasia, spring, summer, and autumn values for NDVI increase in a swath from central Europe through Siberia to the Aldan plateau. In North America, changes in NDVI are spatially fragmented and vary among seasons. The largest increases occur during the spring and summer in the forests of northwestern Canada and Alaska. These same areas show slight declines during the autumn.

[39] To quantify the causes of these changes, we use the regression equations to calculate the change in NDVI associated with temperature, precipitation, SZA, and AOD. The effect of each variable is isolated by simulating the regression equations four times. For each simulation, we change one variable consistent with the historical record while holding the remaining three variables constant. To avoid the effect of extreme values, we calculate the change in the average NDVI between the 1982–1986 period (early 1980s) and the 1995–1999 period (late 1990s). For example, the average anomaly in spring temperature for the grid box in the central Alaska increases by about 2.5°C between the 1982–1986 and 1995–1999 periods. The regression coefficients associated with spring temperature for deciduous broadleaf forests in North America are 0.0079 and −0.0007. These values indicate that the 2.5°C increase in temperature is associated with a 0.02 increase in NDVI. Similar calculations are performed with precipitation, AOD, and SZA to calculate the change in NDVI that is associated with each of these variables for each land cover type and season. The changes in NDVI associated with each of these effects are weighted by the land cover type's fraction of vegetated pixels in that grid box. This allows us to identify the change in NDVI that is associated with changes in temperature, precipitation, AOD, and SZA across North America and Eurasia for spring, summer, and autumn (Figures 3a–3c).

[40] Of the four variables examined, changes in temperature have the greatest explanatory power. Increases in spring temperature have their greatest effect in northwest Canada and central Alaska, where increases in NDVI that are associated with higher temperatures are shown in red (Figure 3a). Conversely, temperature changes reduce autumn NDVI in central Alaska and northwest Canada between the early 1980s and the late 1990s. Higher temperatures also account for some of the summer-time increase in NDVI that stretches across the western portion of Eurasia.

[41] Of the remaining variables, changes in AOD have the greatest effect. The effects of AOD tend to increase NDVI between the early 1980s and late 1990s. This is caused by the periods used for comparison and the timing of volcanic eruptions (Figure 4b). El Chichon erupted in 1982, and its fallout reduced satellite measures of NDVI during the period we define as the early 1980s. Mt. Pinatubo erupted in 1991 and most of its fallout had dissipated by the period we define as the late 1990s, therefore measures of NDVI for the late 1990s are relatively unaffected by reductions in optical depths compared to those for the early 1980s. As a result, changes in the optical properties of the atmosphere cause the GIMMS data set to overstate the change in NDVI between the early 1980s and the late 1990s. But as illustrated in Figures 3a–3c, these changes account for only some of the change in NDVI. Notice too that the effect on NDVI is not constant across longitudes, even though an individual latitudinal band has the same value for AOD. The effects of AOD vary within latitudinal bands due to differences among land cover types regarding the effect of AOD on NDVI (β_6) and changes in the mix of land cover types in grid boxes along the same latitude.

[42] Changes in precipitation account for a relatively small fraction of the change in NDVI. Its effects are scattered across North America and Eurasia (Figures 3a–3c). The observed changes in precipitation tend to decrease NDVI between the early 1980s and late 1990s. These decreases are associated with reductions in precipitation. The small effect of precipitation does not imply that precipitation is unimportant. Rather, it indicates that the change in precipitation between the early 1980s and the late 1990s is relatively small (Figure 4d). This is consistent with a small trend in precipitation relative to the increase in surface temperature at higher latitudes of the northern hemisphere (Figure 4e).

[43] Last, the effects of changes in SZA are nearly invisible during the spring and autumn in both North America and Eurasia (Figures 3a and 3b). The effects in Eurasia are small during the autumn, but are slightly more pronounced during the autumn in North America (Figure 4c).

[44] Consistent with the R^2 of the equations in Tables 2–4, temperature, precipitation, AOD, and SZA account for 10–33% of the spatial and temporal variations in NDVI between 1982 and 1999. Although this percentage does not affect the interpretation of the regression results, it leaves a considerable fraction of the change in NDVI unexplained. As such, this result contradicts *Lucht et al.* [2002], who conclude that temperature is largely responsible for advances timing in the spring green-up, the delay in autumn senescence, and the increase in maximum leaf area index (LAI) observed in satellite images of the northern high latitudes.

[45] The relatively large fraction of unexplained variation may be associated with the use of anomalies. As described in section 2, the use of anomalies eliminates spatial trends in NDVI that are associated with temperature. That is, NDVI increases as latitude decreases, and this increase correlates strongly with the increase in temperature. But this source of variation, and its correlation with temperature, (and hence a larger R^2) is eliminated by the use of anomalies. On the other hand, *Lucht et al.* [2002] use anomalies and seem to explain a larger fraction of the variation.

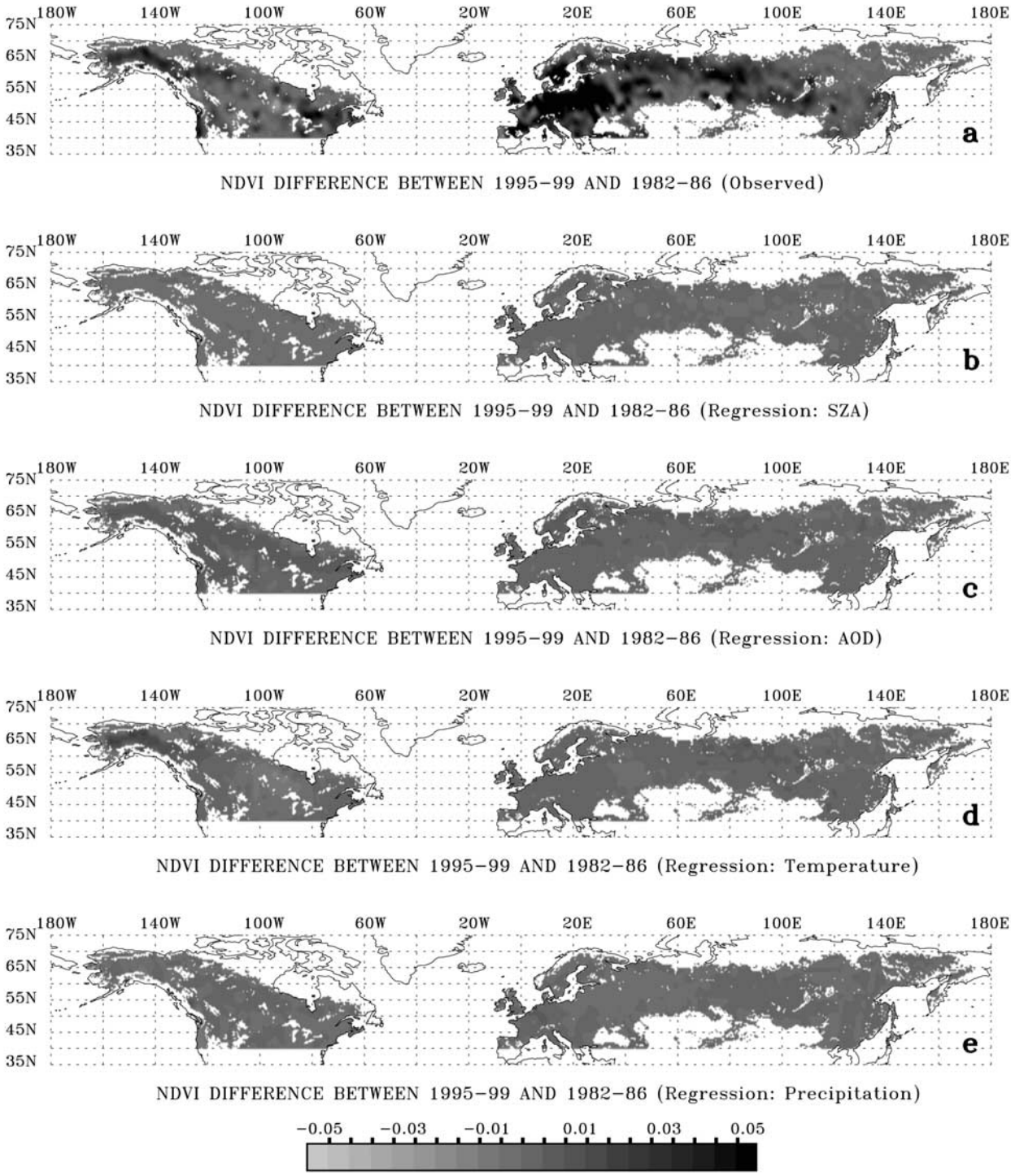

Figure 3a. Spatial patterns of (a) changes in observed NDVI, (b) changes in NDVI due to changes in SZA, (c) changes in NDVI due to changes in AOD, (d) changes in NDVI due to changes in temperature, and (e) changes in NDVI due to changes in precipitation, between 1995–1999 and 1982–1986 averages for land cover types (classes 1–6 in Table 1) during spring. See color version of this figure at back of this issue.

[46] Alternatively, the relatively large fraction of unexplained variation may be associated with the temporal and spatial scale of the analysis. At the continental scale, temperature alone is able to account for 50–90% of the variation in NDVI [*Zhou et al.*, 2001]. Similarly, temperature seems to account for a large fraction of variations in LAI for the boreal zone as indicated by Figure 2 from *Lucht et al.* [2002].

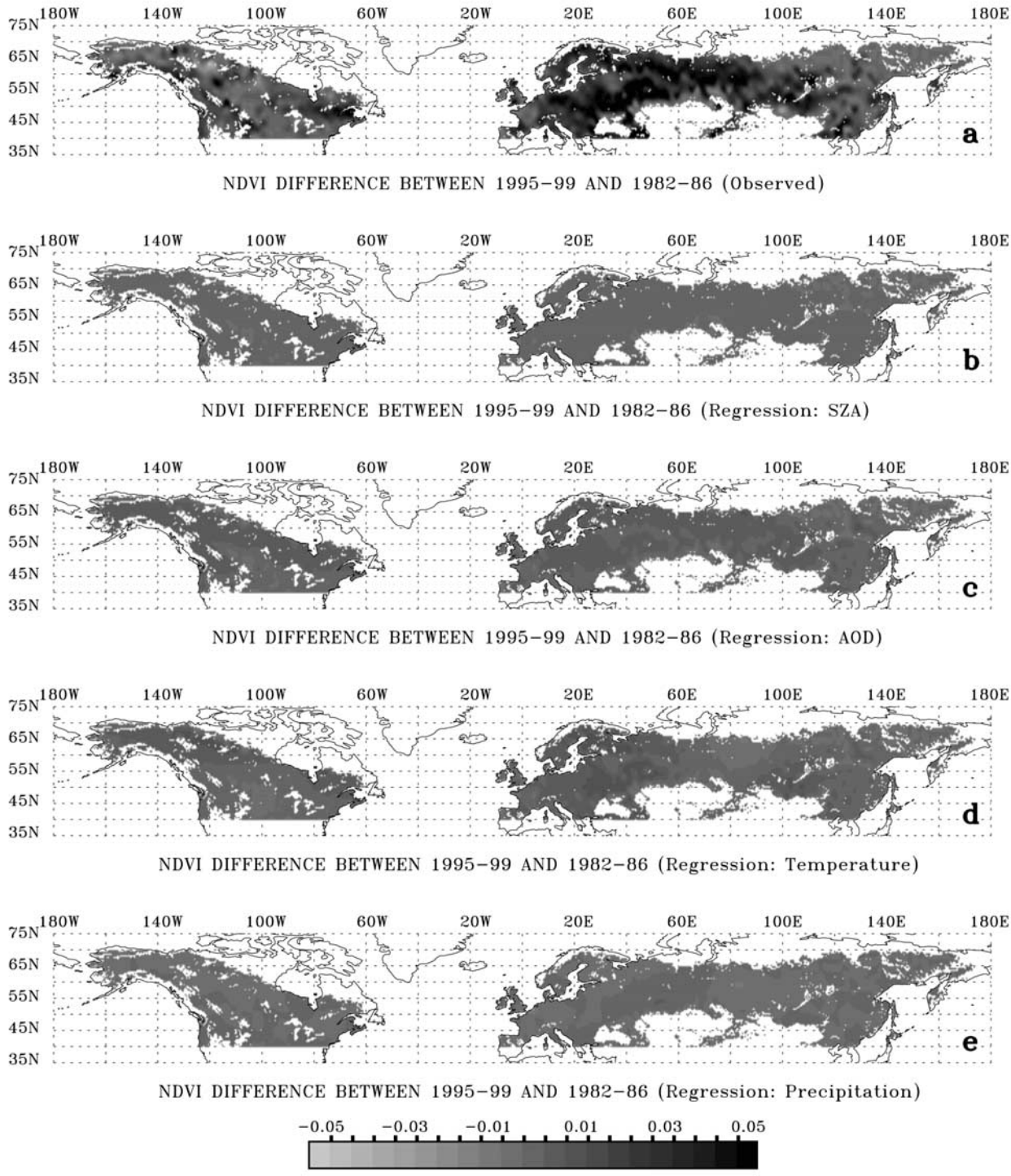

Figure 3b. Same as Figure 3a but for summer. See color version of this figure at back this issue.

[47] To investigate the effect of the temporal and spatial scale on the results of *Lucht et al.* [2002], we estimate the relation between the satellite data and model simulations using the following equation:

$$Sat_t = \alpha + \beta * LPJ_t + \mu_t, \quad (6)$$

in which Sat are the LAI anomalies measured by the satellite at time t and LPJ are the corresponding values simulated by the model. Equation (6) is estimated with the 102 monthly observations and with 18 observations that represent the interannual relation for the growing season and individual months. If the model reproduces the satellite record accurately, $\alpha = 0$ (by definition, the use of anomalies means $\alpha = 0$) and $\beta = 1.0$. If $\beta \neq 1.0$, the model simulations are biased. If $\beta = 0$, the model does not reproduce the satellite data in a statistically meaningful fashion.

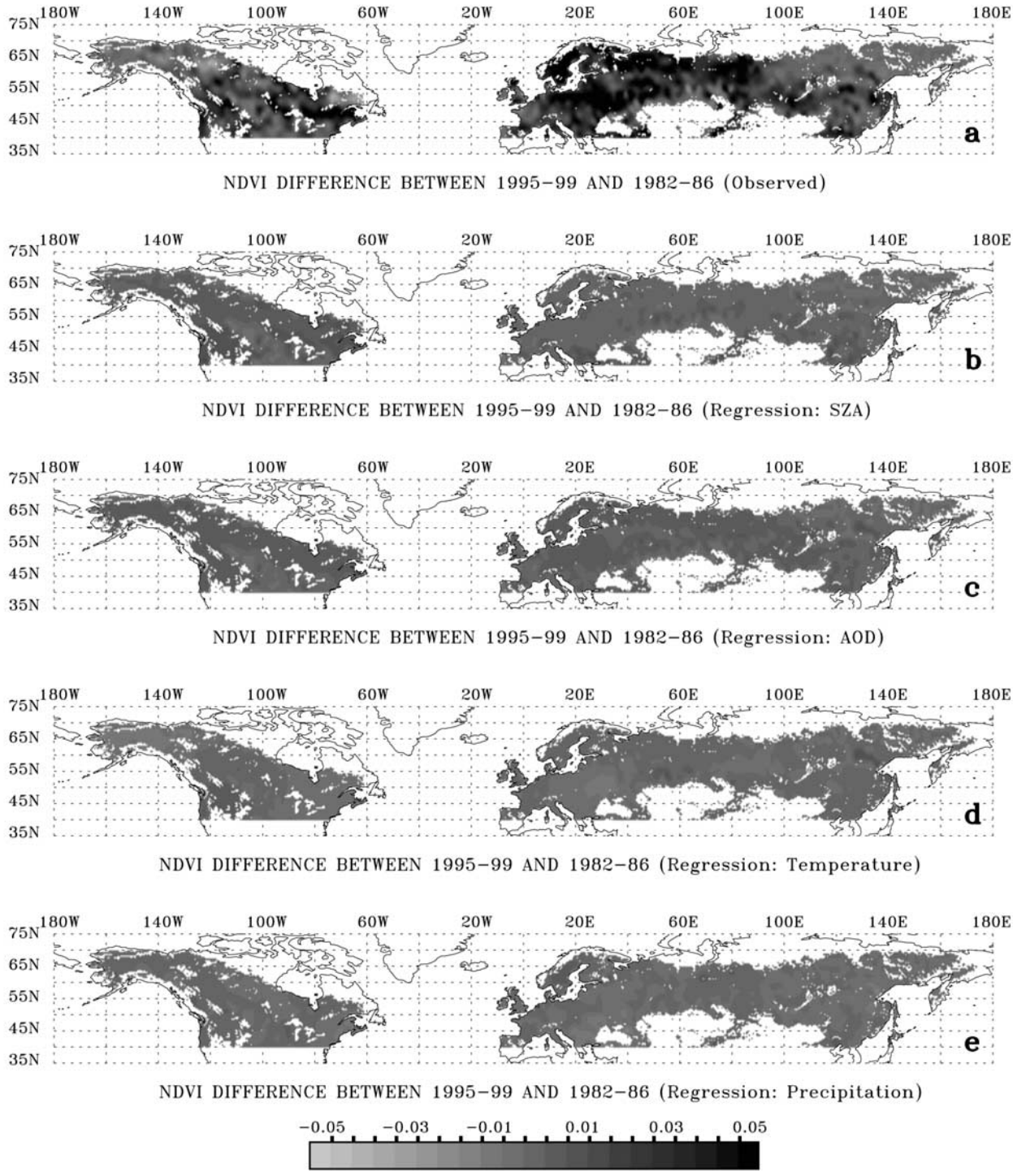

Figure 3c. Same as Figure 3a but for autumn. See color version of this figure at back of this issue.

[48] Results indicate that the regression coefficients are either biased or statistically significant for many months and individual regions (Table 6). These results undermine the conclusions about the effect of temperature on the timing of autumn senescence shown in Figure 2 because there is no statistically meaningful relation between model output and LAI ($\beta = 0$) for September or October in three of the four regression equations. Similarly, the effect of temperature on the timing of spring green-up shown in Figure 2 is clouded by the model's bias for May ($\beta > 1$). Finally, conclusions about the effect of temperature on maximum value of LAI are undermined by the statistical insignificance of regression coefficients for summer August LAI in Northern Europe ($\beta = 0$), where changes

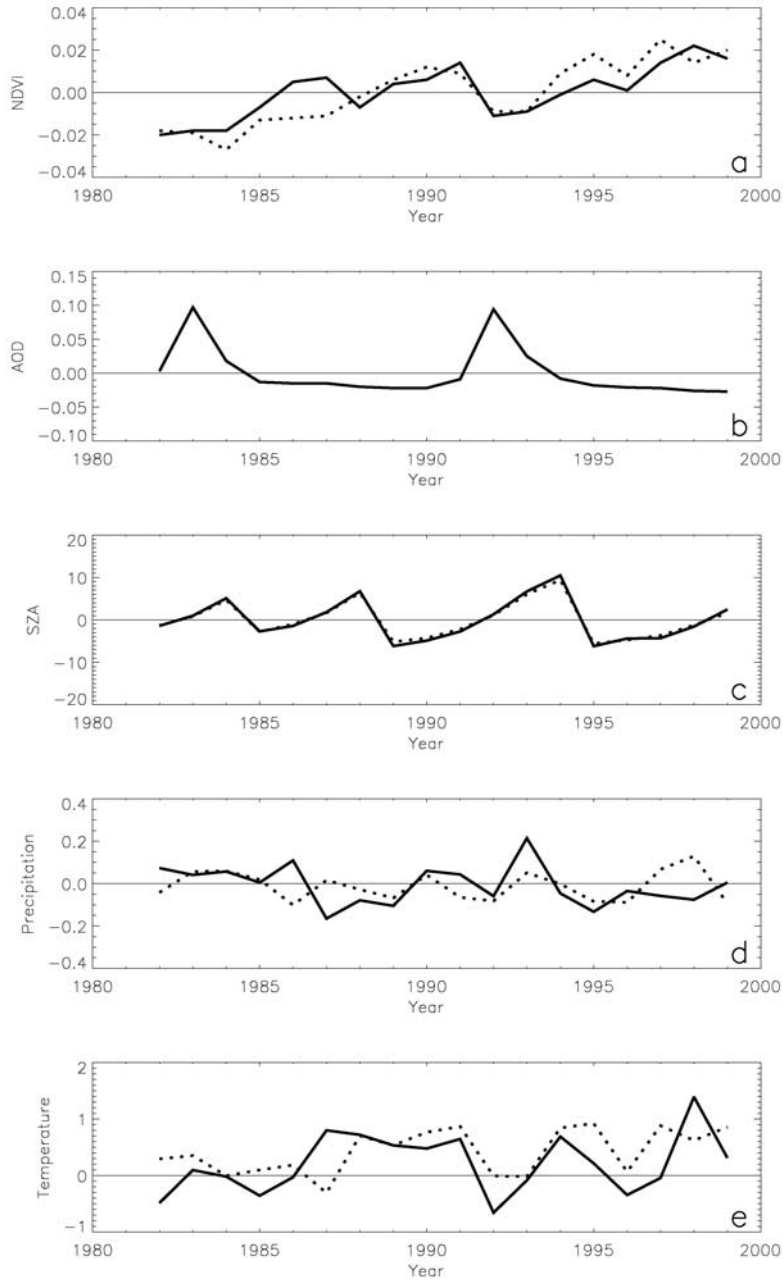

Figure 4. Spatial average of (a) NDVI, (b) AOD, (c) SZA, (d) precipitation, and (e) temperature for vegetated pixels between 40°N and 70°N from 1982 to 1999 in North America (solid line) and Eurasia (dashed line).

in the maximum value of NDVI are greatest [*Zhou et al.*, 2001].

[49] The reason for the relatively low R^2 for the statistical results reported here and the poor performance of the LPJ-DVM at finer temporal and spatial scales may be the omission of important explanatory variables—forest regrowth and changes in land cover and land use. Agricultural abandonment and a slow-down in forest harvest may allow forest to regrow. Changes from barren lands or sparse vegetation to dense vegetation also increase satellite-observed vegetation greenness. These changes would cause NDVI to increase regardless of changes in climate, AOD, or SZA. The importance of forest regrowth is implied by locations where NDVI increases significantly, but the regression equations account for a small portion of the change. This mismatch occurs in the purple areas of northeast and midwest North America and Western Europe east to the Urals. This area coincides with large populations, which implies that human activities have an important effect on land use and land cover.

6. Conclusion

[50] This paper uses satellite-based measures of vegetation greenness to quantify climate-induced changes in terrestrial vegetation. We estimate statistically meaningful

Table 6. Regression Results for Equation (6)

		Monthly	Annual Average	Month					
				5	6	7	8	9	10
Global	β	0.49	1.02	2.99	1.08	0.64	0.91	0.46	1.28
	β = 0	**7.52**	**4.41**	**8.33**	**6.60**	**3.97**	**3.35**	2.04	**2.35**
	β = 1	**7.83**	−0.07	**−5.54**	−0.48	**2.26**	0.35	**2.40**	−0.51
North America	β	0.45	0.66	2.30	0.59	0.48	0.97	0.28	0.86
	β = 0	**5.72**	**3.19**	**6.64**	**4.21**	**2.42**	1.58	1.56	1.92
	β = 1	**6.91**	1.65	**−3.75**	**2.87**	**2.58**	0.06	**3.92**	0.32
Northern Europe	β	0.31	0.33	1.05	0.76	−0.14	0.43	0.32	0.78
	β = 0	**4.09**	0.92	**2.97**	**3.55**	−0.58	0.34	1.23	1.68
	β = 1	**9.15**	1.86	−0.14	1.14	**4.73**	0.45	**2.59**	0.48
Siberia	β	0.52	0.82	2.21	0.79	0.60	0.55	0.20	1.04
	β = 0	**6.59**	**4.33**	**10.5**	**5.78**	**3.81**	**2.35**	0.94	1.96
	β = 1	**6.09**	0.95	**−5.72**	1.55	**2.51**	1.93	**3.69**	−0.08

Values that exceed the $p < 0.05$ threshold in bold.

relations between NDVI and climate during spring, summer, and autumn for forests between 40°N and 70°N in North America and Eurasia by land cover type at a regional scale (2° × 2° grid boxes) between 1982 and 1999. The results indicate that temperature changes between the early 1980s and the late 1990s are linked with much of the observed increase in satellite measures of northern forest greenness. But a statistical meaningful relation does not imply causation. Indeed, physical theory indicates that two directions of causality are possible. There are ecological and physical mechanisms by which climate can affect plant growth and there are physical and ecological mechanisms by which plant growth can affect climate.

[51] In mid and high latitudes, climate affects the productivity of forest ecosystems directly through temperature and precipitation [e.g., *Chapin and Shaver*, 1996]. In general, warm temperatures and high rainfall increase rates of plant photosynthesis because photosynthesis is enhanced by higher temperatures and greater stomatal conductance [*Kramer*, 1982].

[52] Climate affects the productivity of terrestrial ecosystems indirectly through changes in nutrient availability. Higher air temperatures tend to increase soil temperatures, which accelerate the decomposition of organic matter and nutrient release [*Nadelhoffer et al.*, 1991] and therefore productivity. The indirect effect of warming on nutrient availability ultimately may drive the productivity response of mid- and high-latitude forests because nutrients limit net primary production over wide areas of these ecosystems [*McKendrick et al.*, 1978; *Shaver and Chapin*, 1980; *Shaver et al.*, 1986].

[53] Warming in high latitude forests also may affect terrestrial productivity in the short term (from years to decades) by changing the physiological function and the morphology of the extant plant community, and in the long-term (from decades to centuries) by changing species composition [*Schlesinger*, 1997]. The direct, short-term effects of warming on the extant plant community include earlier leaf expansion [*Chapin and Shaver*, 1996] and shifts in phenology [*Myneni et al.*, 1997], as well as increases in the rate of photosynthesis, shoot elongation, and leaf turnover [*Chapin and Shaver*, 1996]. In the longer term, changing climate may affect productivity by altering species composition. These effects probably are small due to the relatively short 20-year sample period.

[54] Changes in the structure and function of terrestrial ecosystems may influence the climate system via the exchange of heat, moisture, trace gases, aerosols, and momentum between land surfaces and the overlying air [*Pielke et al.*, 1998]. The effect of temperature and precipitation is created by the vegetation's interception of total radiative flux that reaches the Earth's surface. This interception modifies the amount of available net radiant energy via its effect on albedo, and changes the partitioning between sensible and latent heat via its effect on canopy transpiration and aerodynamic roughness.

[55] Consistent with these effects, modeling studies generally indicate that increases in vegetation lower temperature and increase precipitation. *Nobre et al.* [1991] find that replacing the tropical forests in the Amazon basin with pasture increases temperature by about 2.5°K and reduces precipitation by 2.5 percent. Changes in vegetation need not be so extreme. Analyses indicate regional changes in LAI generate regional changes in temperature and precipitation that are consistent with the effects described above [*Bounoua et al.*, 2000; *Buermann et al.*, 2001]. Empirical studies also indicate that vegetation affects temperature and precipitation. *Schwartz and Karl* [1990] find that the emergence of leaves in the eastern US reduces daily surface maximum temperatures by 1.5°C–3.5°C. Measurements of weather variables in an intact forest and the pasture of a cattle ranch indicate that maximum temperatures are greater in the cleared area, especially during the dry season when the lack of water slows transpiration [*Bastable et al.*, 1993]. Because of the simultaneous relation between climate and vegetation, future study will use statistical techniques that can identify the presence and direction of causal relations.

[56] Warming-enhanced plant growth in northern forests also may affect the terrestrial carbon cycle. Increased plant growth is linked to changes in biomass [*Myneni et al.*, 2001], which suggests that climate induced increases in NDVI may increase in terrestrial biomass (as opposed to carbon stored in soils about which our analysis says nothing), which could account for some of the missing carbon. The possibility of a temperature mediated terrestrial sink for carbon is consistent with a statistical analysis of the time series for carbon uptake by the unknown carbon sink (R. K. Kaufmann and J. H. Stock, Testify hypotheses about the unknown carbon sinks: A time series anaysis, submitted to *Global Biogeochemical Cycles*, 2002). They find that the

annual variations in the time series for the unknown carbon sink are associated with annual variations in land surface temperature in the northern hemisphere, as opposed to land surface temperature in the southern hemisphere or sea surface temperature in either hemisphere. They also find that the time series for the unknown carbon sink is related to summer temperature, as opposed to temperature in the winter, spring, or autumn. This is consistent with our finding that temperature has its greatest effect on NDVI in North America and Eurasia during the summer (Figures 3a–3c). Together, these results imply that changes in climate may have stimulated the terrestrial vegetation in mid- to high-latitude forests to increase their uptake of carbon and that this increase may account for some of the missing carbon.

Appendix A

A1. Specification Tests

[57] The procedure to chose among equations (3), (4), and (5) is based on *F* tests that compare their residual sum of squares (RSS). RSS is the sum of the squared errors from the regression equation ($\sum \varepsilon_{sit}^2$). We test the null hypothesis that the slopes and intercepts are the same for each grid box by calculating the following *F* statistic,

$$F_3 = \frac{(RSS_3 - RSS_5)/[(N-1)K]}{RSS_5/[NT - N(K+1)]}, \quad (A1)$$

in which RSS_3 is the residual sum of squares from equation (3), RSS_5 is the residual sum of squares for equation (5), N is the number of grid boxes for a particular land cover type, T is the number of observations per grid box (18), and K is the number of regression coefficients. If the slopes and intercepts differ significantly among grid boxes, equation (5) will fit the data more closely than equation (3). Under these conditions, RSS_3 will be much larger than RSS_5, the value of the *F* statistic will exceed the critical value ($p < 0.05$), and we will reject the null hypothesis that the slopes and intercepts are equal. Failure to reject this null indicates that the intercept and slopes are the same across grid boxes and that equation (3) can be used to estimate the relation between NDVI and climate.

[58] Equation (3) is not appropriate if the null hypothesis is rejected. In this case, we test whether differences in the intercepts are responsible for the large residual sum of squares for equation (3) relative to equation (5). To test the null hypothesis that the intercepts differ among grid boxes (i.e., the α's differ), but the relations between NDVI and the climate variables are the same (i.e., the β's are the same), we calculate the following *F* statistic,

$$F_1 = \frac{(RSS_4 - RSS_5)/[(N-1)K]}{RSS_5/[NT - N(K+1)]}, \quad (A2)$$

in which RSS_4 is the residual sum of squares from equation (4). If the relations between NDVI and individual climate variables vary among grid boxes, equation (5) will fit the data more closely than equation (4). Under these conditions, RSS_4 will be much larger than RSS_5, the value of the *F* statistic will exceed the critical value ($p < 0.05$), and we will reject the null hypothesis that the slopes are equal. Rejecting the null hypothesis indicates that the relation between NDVI and climate should be estimated using equation (5). Failure to reject this null (equation (A2)) combined with rejecting the null hypothesis that the slopes and the intercepts are the same across grid boxes (equation (A1)) indicates that the intercepts vary among grid boxes but the slopes are the same. Under these conditions, equation (4) can be used to estimate the relation between NDVI and climate.

[59] Once equation (3), (4), or (5) is chosen, each requires a different estimation technique. Equation (3) can be estimated using ordinary least squares (OLS). The nature of the data (time series for many grid boxes) implies that the variance of the error term (ε) may not be constant (i.e. heteroscedactic). Heteroscedasticity does not bias the estimates for the regression coefficients, but may reduce the efficiency of the estimate. The loss of efficiency implies that the standard errors associated with the regression coefficients are too large. This would cause us to understate the statistical significance of the estimates for α and the β's.

[60] The error term is tested for heteroscedasticity using a test developed by *Breusch and Pagan* [1979]. The test evaluates whether the absolute size of the error term from equation (3) is related to the absolute size of the dependent or independent variables. The R^2 of this regression times the number of observations (N * T) is used as a test statistic that is distributed as a χ^2 with degrees of freedom equal to the number of independent variables plus 1. This statistic tests the null hypothesis that the variance of the error term is constant. Values of the test statistic that exceed the critical threshold ($p < 0.05$) indicate that the r squared of the relation between the error term and the dependent and independent variables is larger than would be expected based on random chance. Such a result (i.e. rejecting the null) indicates that the error term is heteroscedactic.

[61] The inefficiency associated with a heteroscedactic error term can be alleviated two ways. Weighted least squares can eliminate the heteroscadasticity if the cause of heteroscadasticity is known. One possible cause for a heteroscedactic error in equation (3) are differences among grid boxes regarding the number of pixels associated with a given land cover type. For example, the number of pixels classified as evergreen needleleaf forests (class 1) per grid box in Eurasia varies between 6 and 2,298. Boxes with relatively few pixels may sample the relation between NDVI and climate differently than the sample derived from grid boxes with many pixels, and this difference may cause the error from equation (3) to be heteroscedactic. To account for this effect, we weight the observations by the number of pixels per grid box. This regression result is termed the weighted least squares estimator (WLS). The errors from the WLS estimate are tested for heteroscedasticity using the test developed by *Breusch and Pagan* [1979]. If the test indicates that the WLS error term is heteroscedactic, we use the procedure developed by *Newey and West* [1987] to calculate a heteroscedasticity and autocorrelation consistent covariance matrix. This matrix is used to calculate standard errors that evaluate the statistical significance of the regression coefficients efficiently. This result for equation (3) is termed the heteroscedactic and autocorrelation consistent (HAC) estimate.

[62] If the *F* tests indicate that only the intercepts vary among grid boxes, this specification (equation (4)) can be estimated using either the fixed or the random effects

estimator. These estimators differ according to the way in which they weight the relation between NDVI and independent variables within grid boxes relative to the way in which they weight the relation between NDVI and independent variables between grid boxes. The fixed effects estimator examines the relation between NDVI and independent variables within grid boxes only. To do so, the fixed effects estimator subtracts the mean value for each variable for each grid box. As a result, the mean value for each variable for each grid box is zero. Under these conditions, there is no variation among grid boxes. Without this component of variation, the fixed effects estimator for the β's in equation (4) represents the relation between NDVI and independent variables based on the relation that exists within grid boxes only.

[63] To include information about the relation between NDVI and independent variables that is contained in the between group variation, the error term from equation (3) can be decomposed into three components

$$\mathrm{NDVI}_{sit} = \alpha + \sum_{s=0}^{-2} \left(\beta_{s1}\mathrm{Temp}_{sit} + \beta_{s2}\mathrm{Temp}_{sit}^2 + \beta_{s3}\mathrm{Prec}_{sit} + \beta_{s4}\mathrm{Prec}_{sit}^2\right) + \beta_{s5}\mathrm{SZA}_{it} + \beta_{s6}\mathrm{AOD}_{it} + \varepsilon_{si} + \varepsilon_{sr} + \varepsilon_{st}, \quad \text{(A3)}$$

where ε_{si} is a time invariant component of the error term that is associated with grid box i, ε_{sr} is component of the error term that varies over among individuals and across time (the random component), and ε_{st} is the component of the error term that varies over time but is the same for all grid boxes at any time. Using the ε_{si} component to represent differences among grid boxes allows the random effects estimator to include both the within and between group variation in its estimate for the relation between NDVI and climate. The between group relation between NDVI and the explanatory variables is that which would be estimated from variations in the 18 year mean value of NDVI and the explanatory variables from each of the grid boxes. The random effects estimator weights the within and between group relations, using well defined statistical procedures [*Hsiao*, 1986].

[64] The ability of the random effects estimator to use both the within and between group relation between NDVI and explanatory variables is based on the assumption that there is no correlation between the intercepts for individual grid boxes and the size of the explanatory variables (i.e. climate variables). In other words, there is no relation between a grid box's temperature or precipitation anomalies and its intercept. This assumption is tested to choose between the fixed or random effects estimator. The fixed effects estimator is appropriate if a test statistic developed by *Hausman* [1978] or *Mundlak* [1978] rejects the null hypothesis that there is no relation between the size of explanatory variables and the intercepts for individual grid boxes.

[65] If the *F* tests indicate that both the intercepts and slopes vary among grid boxes (it makes no sense that the intercepts are the same across grid boxes but the slopes vary), we estimate equation (5) using the random coefficient model. The random coefficient model is based on the assumption that the value of β_i for any grid box is equal to a mean value for all grid boxes (β) plus or minus some random error (λ_i),

$$\beta_i = \beta + \lambda_i. \quad \text{(A4)}$$

[66] *Swamy* [1970] describes a method for estimating both the mean value for β and its variance. Using this technique, we can estimate the relation between NDVI and climate while allowing this relation to vary among the grid boxes. This estimate of equation (5) is termed the random coefficient model (RCM).

[67] **Acknowledgments.** This work was funded by the NASA Earth Science Enterprise and the NOAA Office of Global Programs. We would like to thank J. Hansen for making the station temperature data accessible.

References

Asrar, G., M. Fuchs, E. T. Kanemasu, and J. L. Hatfield, Estimation absorbed photosynthetic radiation and leaf area index from spectral reflectance in wheat, *Agron. J.*, *76*, 300–306, 1984.

Bastable, H. G., W. J. Shuttleworth, R. L. G. Dallarosa, G. Fisch, and C. A. Nobre, Observations of climate albedo, and surface radiation over cleared and undisturbed Amazonian forest, *Int. J. Climatol.*, *12*, 783–796, 1993.

Bounoua, G. J., G. J. Collartz, S. O. Los, P. J. Sellers, D. A. Dazlich, C. J. Tucker, and D. Randall, Sensitivity of climate to changes in NDVI, *J. Clim.*, *13*, 2277–2292, 2000.

Braswell, B. H., D. S. Schimel, E. Linder, and B. Moore, The response of global terrestrial ecosystems to interannual temperature variability, *Science*, *278*, 870–872, 1997.

Breusch, T. S., and A. R. Pagan, A simple test for heteroscedasticity and random coefficient variation, *Econometrica*, *47*, 1287–1294, 1979.

Buermann, W., J. Dong, Z. Zeng, R. B. Myneni, and R. E. Dickinson, Evaluation of the utility of satellite-based vegetation leaf area index data for climate simulations, *J. Clim.*, *14*, 3536–3550, 2001.

Chapin, F. S., and G. R. Shaver, Physiological and growth responses of Arctic plants to a field experiment simulating climatic change, *Ecology*, *77*, 822–840, 1996.

Cihlar, J., St. Laurent, and J. A. Dyer, The relation between normalized difference vegetation index and ecological variables, *Remote Sens. Environ.*, *35*, 279–298, 1991.

DeFries, R., M. Hansen, J. Townshend, and R. Sohlberg, Global land cover classification at 8km spatial resolution: The use of training data derived from LANDSAT imagery in decision tree classifiers, *Int. J. Remote Sens.*, *19*, 3141–3168, 1998.

Easterling, D. R., T. R. Karl, and K. P. Gallo, Observed climate variability and change of relevance to the biosphere, *J. Geophys. Res.*, *105*, 20,101–20,114, 2000.

Gates, D. M., *Climate Change and Its Biological Consequences*, Sinauer Associates, Sunderland, Mass., 1993.

Goward, S. N., and S. D. Prince, Transient effects of climate on vegetation dynamics: Satellite observations, *J. Biogeogr.*, *22*, 549–563, 1995.

Groisman, P. Y., T. R. Karl, and R. W. Knight, Observed impact of snow cover on the heat balance and the rise of continent spring temperature, *Science*, *263*, 198–200, 1994.

Gutman, G., On the use of long-term global data of land reflectances and vegetation indices derived from the advanced very high resolution radiometer, *J. Geophys. Res.*, *104*, 6241–6255, 1999.

Hansen, J., R. Ruedy, J. Glascoe, and M. Sato, GISS analysis of surface temperature change, *J. Geophys. Res.*, *104*, 30,997–31,022, 1999.

Hausman, J. A., Specification test in econometrics, *Econometrica*, *46*, 1251–1271, 1978.

Holben, B. N., Characteristics of maximum value compositing imagines for AVHRR data, *Int. J. Remote Sens.*, *7*, 1417–1437, 1986.

Hsiao, C., *Analysis of Panel Data*, Cambridge Univ. Press, New York, 1986.

Huemmrich, K. F., T. A. Black, P. G. Jarvis, J. H. McCaughey, and F. G. Hall, High temporal resolution NDVI phenology from micrometeorological radiation sensors, *J. Geophys. Res.*, *104*, 27,935–27,944, 1999.

IPCC, *Climate Change 2001: The Scientific Basis*, edited by D. L. Albritton, et al., Cambridge Univ. Press, New York, 2001.

Kao, C., Spurious regression and residual-based tests for cointegration in panel data, *J. Econometrics*, *90*, 1–44, 1999.

Kaufmann, R. K., and S. Snell, A biophysical model of corn yield: Integrating physical and economic determinants, *Am. J. Agric. Econ.*, *79*(1), 178–180, 1997.

Kaufmann, R. K., L. Zhou, Y. Knyazikhin, N. Shabanov, R. Myneni, and C. Tucker, Effect of orbital drift and sensor changes on the time series of AVHRR vegetation index data, *IEEE Trans. Geosci. Remote Sens.*, *38*, 2584–2597, 2000.

Keeling, C. D., T. P. Whorf, M. Wahlen, and J. van der Pilcht, Interannual extremes in the rate of rise of atmospheric carbon dioxide since 1990, *Nature*, *375*, 666–670, 1995.

Keeling, C. D., J. F. S. Chin, and T. P. Whorf, Increased activity of northern vegetation inferred from atmospheric CO_2 measurements, *Nature*, *382*, 146–149, 1996.

Kramer, P. J., Water and plant productivity of yield, in *Handbook of Agricultural Productivity*, edited by M. Rechcigl, pp. 41–47, CRC Press, Boca Raton, Fla., 1982.

Larcher, *Physiological plant Ecology*, 2nd edn., Spring-Verlag, Berlin, 1983.

Los, S. O., Estimation of the ratio of sensor degradation between NOAA AVHRR channels 1 and 2 from monthly NDVI composites, *IEEE Trans. Geosci. Remote Sens.*, *36*, 202–213, 1998.

Lucht, W., L. C. Prentice, R. B. Myneni, S. Sitch, P. Friedlingstein, W. Cramer, P. Bousquet, W. Buermann, and B. Smith, Climatic control of the high-latitude vegetation greening trend and Pinatubo effect, *Science*, *296*, 1687–1689, 2002.

McKendrick, J. D., V. J. Ott, and G. A. Mitchell, Effects of nitrogen and phosphorus fertilization on carbohydrate and nutrient levels in *Dupontia fisheri* and *Acrtagrostis latifolia*, in *Vegetation and Production Ecology of an Alaskan Arctic Tundra*, edited by L. L. Tiesen, pp. 509–537, Springer-Verlag, New York, 1978.

Melillo, J. M., A. D. McGuire, D. W. Kicklighter, B. Moore, C. J. Vorosmarty, and A. L. Schloss, Global climate change and terrestrial net primary production, *Nature*, *363*, 234–240, 1993.

Mundlak, Y., On the pooling of time series and cross section data, *Econometrica*, *46*, 69–85, 1978.

Myneni, R. B., F. G. Hall, P. J. Sellers, and A. L. Marshak, The interpretation of spectral vegetation indexes, *IEEE Trans. Remote Sens.*, *33*, 481–486, 1995.

Myneni, R. B., S. O. Los, and C. J. Tucker, Satellite-based identification of linked vegetation index and sea surface temperature anomaly areas from 1982–1990 for Africa, Australia and South America, *Geophys. Res. Lett.*, *23*, 729–732, 1996.

Myneni, R. B., C. D. Keeling, C. J. Tucker, G. Asrar, and R. R. Nemani, Increased plant growth in the northern high latitudes from 1981–1991, *Nature*, *386*, 698–702, 1997.

Myneni, R. B, J. Dong, C. J. Tucker, R. K. Kaufmann, P. E. Kauppi, J. Liski, L. Zhou, V. Alexeyev, and M. K. Huges, A large carbon sink in the woody biomass of northern forests, *Proc. Natl. Acad. Sci. U. S. A.*, *98*(26), 14,784–14,789, 2001.

Nadelhoffer, K. J., A. E. Giblin, G. R. Shaver, and J. A. Laundre, Effects of temperature and substrate quality on element fertilization in six arctic soils, *Ecology*, *72*, 242–253, 1991.

Nemani, R., M. White, P. Thornton, K. Nishida, S. Reddy, J. Jenkins, and S. Running, Recent trends in hydrological balance have enhanced the terrestrial carbon sink in the United States, *Geophys. Res. Lett.*, *29*(10), 1468, doi:10.1029/2002GL014867, 2002.

Newey, W., and K. West, A simple positive-definite heteroskedasticity and autocorrelation consistent matrix, *Econometrica*, *55*, 703–708, 1987.

Nobre, C., P. J. Sellers, and J. Shukla, Amazonian deforestation and regional climate change, *J. Clim.*, *4*, 957–988, 1991.

Peterson, T. C., and R. S. Vose, An overview of the Global Historical Climatology Network temperature database, *Bull. Am. Meteorol. Soc.*, *78*, 2837–2849, 1997.

Pielke, R. A., R. Avissar, M. Raupach, A. J. Dolman, X. Zeng, and A. S. Denning, Interactions between the atmosphere and terrestrial ecosystems: Influence on weather and climate, *Global Change Biol.*, *4*, 461–475, 1998.

Randerson, J. T., C. B. Field, I. Y. Fung, and P. P. Tans, Increases in early season ecosystem uptake explain recent changes in the seasonal cycle of atmospheric CO_2 at high northern latitudes, *Geophys. Res. Lett.*, *26*, 2765–2769, 1999.

Sato, M., J. E. Hansen, M. P. McCormick, and J. B. Pollack, Stratospheric aerosol optical depth, 1850–1990, *J. Geophys. Res.*, *98*, 22,987–22,994, 1993.

Schlesinger, W. H., *Biogeochemistry: An Analysis of Global Change*, Academic, San Diego, Calif., 1997.

Schultz, P. A., and M. S. Halpert, Global correlation of temperature, NDVI and precipitation, *Adv. Space Res.*, *13*, 277–280, 1993.

Schwartz, M. D., and T. R. Karl, Spring phenology: Nature's experiment to detect the effect of "green-up" on surface maximum temperature, *Mon. Weather Rev.*, *118*, 883–8890, 1990.

Shaver, G. R., and F. S. Chapin III, Response to fertilization by various plant growth forms in an Alaskan tundra: Nutrient accumulation and growth, *Ecology*, *61*, 662–675, 1980.

Shaver, G. R., F. S. Chapin, and B. L. Gartner, Factors limiting seasonal growth and peak biomass accumulation in *Eriophorum vaginatum* in Alaskan tussoc tundra, *J. Ecol.*, *74*, 257–278, 1986.

Swamy, P. A. V. B., Efficient inference in a random coefficient regression model, *Econometrica*, *38*, 311–323, 1970.

Tucker, C. J., W. W. Newcomb, and H. E. Dregne, AVHRR data sets for determination of desert spatial extent, *Int. J. Remote Sens.*, *15*, 3547–3565, 1994.

Vermote, E. E., and N. Z. El Saleous, Statospheric aerosol perturbing effect on remote sensing of vegetation: Operational method for the correction of AVHRR composite NDVI, *SPIE Atmos. Sens. Model.*, *2311*, 19, 1994.

Vermote, E. F., and Y. J. Kaufman, Absolute calibration of AVHRR visible and near-infrared channels using ocean and cloud views, *Int. J. Remote Sens.*, *16*, 2317–2340, 1995.

Vinnikov, K. Y., A. Robock, R. J. Stouffer, J. E. Walsh, C. L. Parkinson, D. J. Cavalieri, J. F. B. Mitchell, D. Garrett, and V. F. Zakharov, Global warming and Northern Hemisphere sea ice extent, *Science*, *286*, 1934–1937, 1999.

Xie, P., and P. A. Arkin, Global Precipitation: A 17-year monthly analysis based on gauge observations, satellite estimates and numerical model outputs, *Bull. Am. Meteorol. Soc.*, *78*, 2539–2558, 1997.

Zhou, L., C. J. Tucker, R. K. Kaufmann, D. Slayback, N. V. Shabanov, and R. B. Myneni, Variations in northern vegetation activity inferred from satellite data of vegetation index during 1981 to 1999, *J. Geophys. Res.*, *106*, 20,069–20,083, 2001.

R. K. Kaufmann and R. B. Myneni, Department of Geography, Boston University, Boston, MA 02215, USA.

Y. Tian and L. Zhou, School of Earth and Atmospheric Sciences, Georgia Institute of Technology, 221 Bobby Dodd Way, Atlanta, GA 30332, USA. (lmzhou@eas.gatech.edu)

C. J. Tucker, Biospheric Sciences Branch, Code 923, NASA Goddard Space Flight Center, Greenbelt, MD 20771, USA.

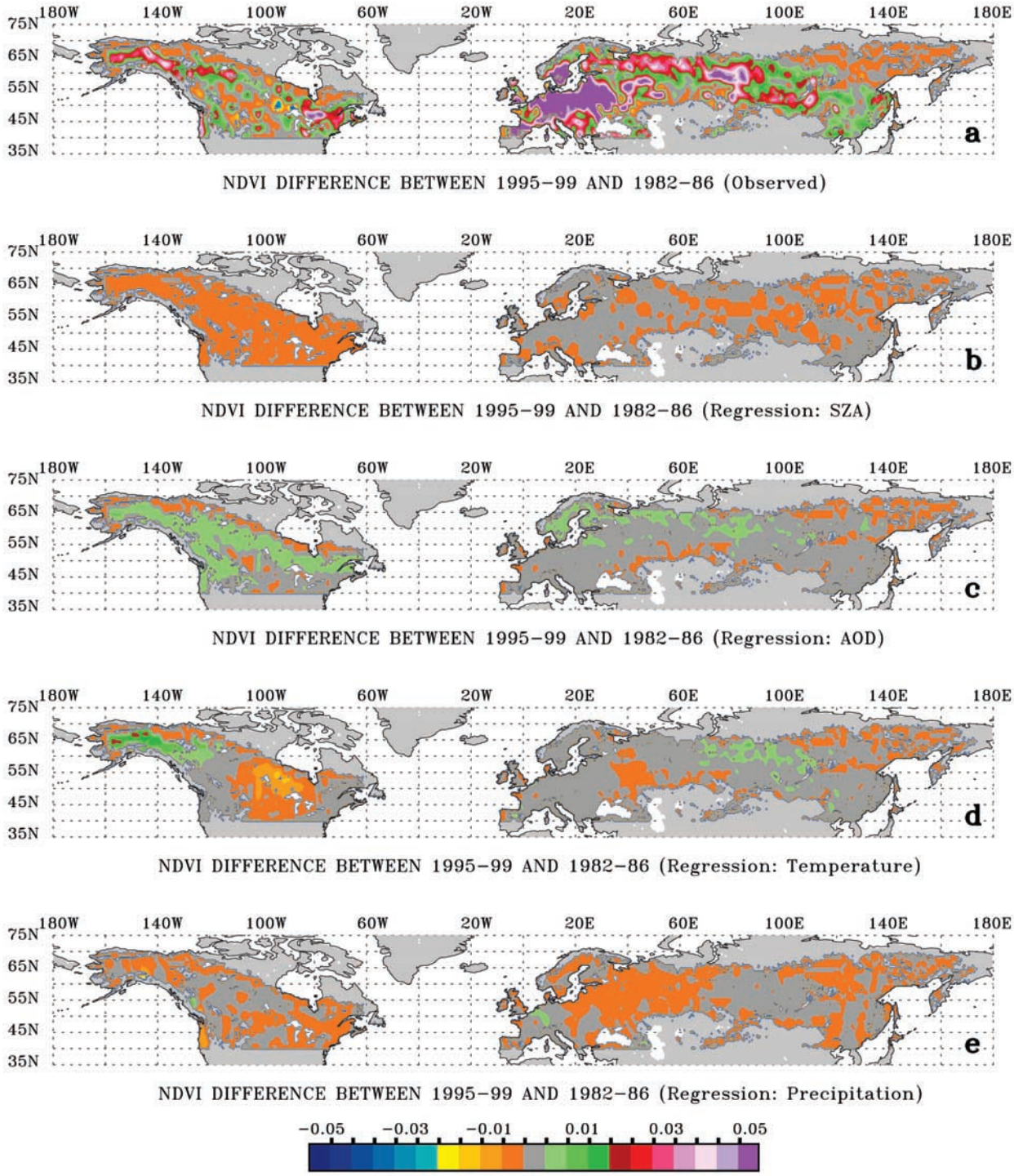

Figure 3a. Spatial patterns of (a) changes in observed NDVI, (b) changes in NDVI due to changes in SZA, (c) changes in NDVI due to changes in AOD, (d) changes in NDVI due to changes in temperature, and (e) changes in NDVI due to changes in precipitation, between 1995–1999 and 1982–1986 averages for land cover types (classes 1–6 in Table 1) during spring.

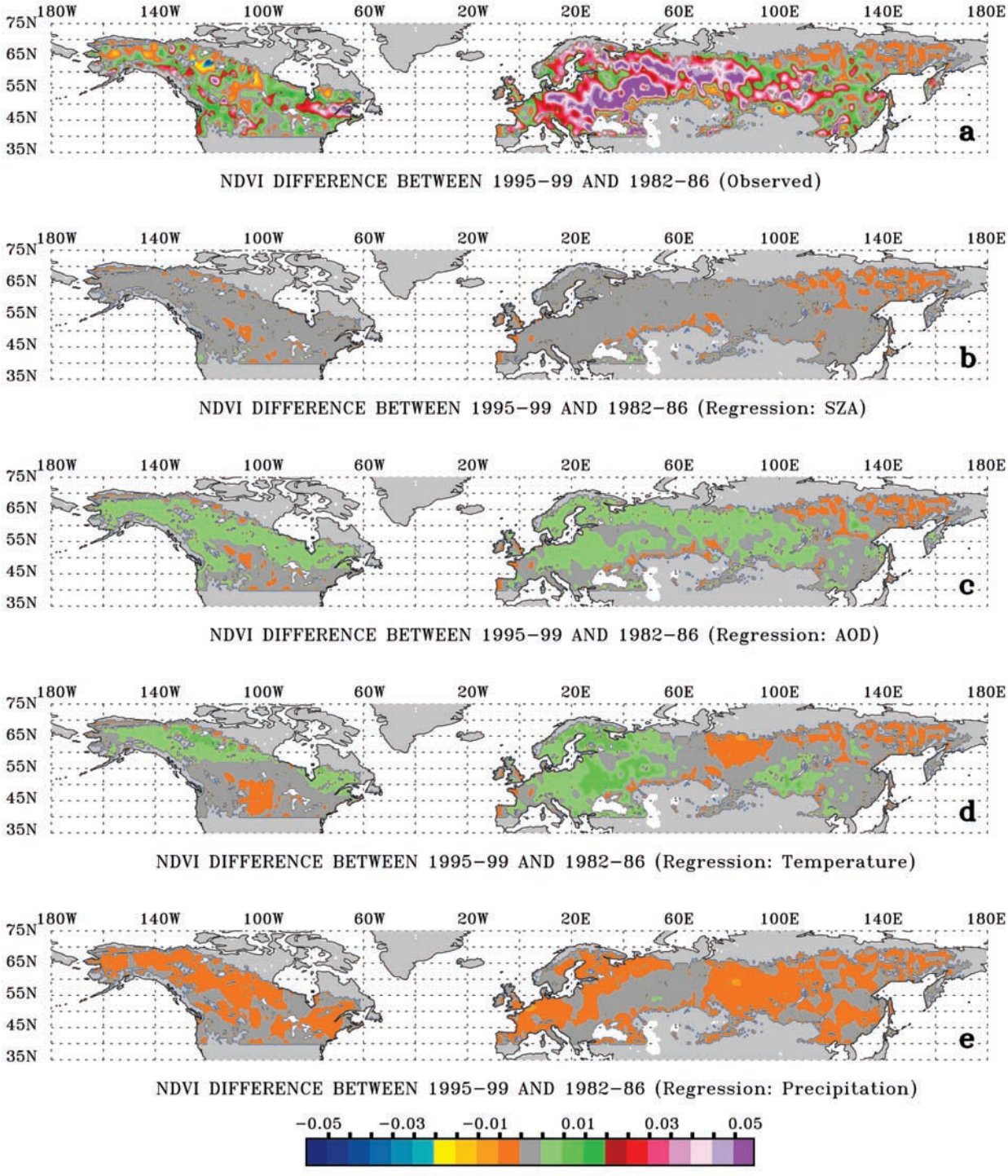

Figure 3b. Same as Figure 3a but for summer.

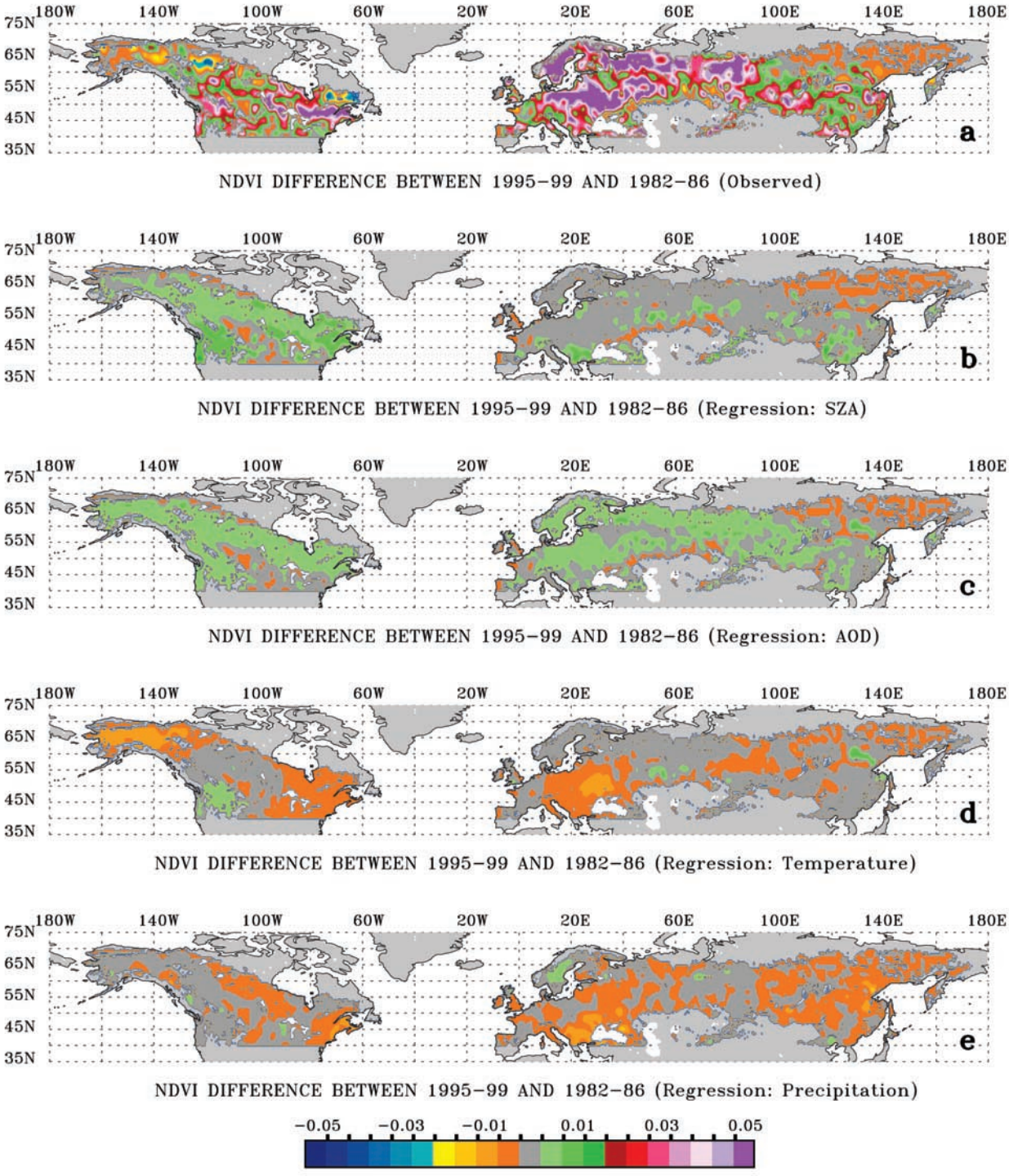

Figure 3c. Same as Figure 3a but for autumn.